

# XCloud-MoDern: An Artificial Intelligence Cloud for Accelerated NMR Spectroscopy

Zi Wang,<sup>[a]</sup> Di Guo,<sup>[b]</sup> Zhangren Tu,<sup>[b]</sup> Yihui Huang,<sup>[a]</sup> Yirong Zhou,<sup>[a]</sup> Jian Wang,<sup>[a]</sup> Liubin Feng,<sup>[c]</sup> Donghai Lin,<sup>[c]</sup> Yongfu You,<sup>[d]</sup> Tatiana Agback,<sup>[e]</sup> Vladislav Orekhov,<sup>[f]</sup> Xiaobo Qu<sup>\*[a]</sup>

**Abstract:** For accelerated multi-dimensional NMR spectroscopy, non-uniform sampling is a powerful approach but requires sophisticated algorithms to reconstruct undersampled data. Here, we first devise a high-performance deep learning framework (MoDern), which shows astonishing performance in robust and high-quality reconstruction of challenging multi-dimensional protein NMR spectra and reliable quantitative measure of the metabolite mixture. Remarkably, the few trainable parameters of MoDern allowed the neural network to be trained on solely synthetic data while generalizing well to experimental undersampled data in various scenarios. Then, we develop a novel artificial intelligence cloud computing platform (XCloud-MoDern), as a reliable, widely-available, ultra-fast, and easy-to-use technique for highly accelerated NMR. All results demonstrate that XCloud-MoDern contributes a promising platform for further development of spectra analysis.

NMR spectroscopy serves as an indispensable biophysical tool in modern chemistry, biology, and life science. Since the duration of an NMR experiment increases rapidly with the dimensionality and spectral resolution, accelerating the data acquisition by using the non-uniform sampling (NUS) approach<sup>[1]</sup> becomes widely accepted practice. Over the past two decades, many methods have been established in the NMR field to reconstruct high-quality spectra from NUS data. The two main strategies are model-based optimization<sup>[2]</sup> and data-driven deep learning<sup>[3]</sup>.

For model-based optimization methods, they are well theoretically grounded and has specific priors with insights from NMR spectroscopy. A range of modern approaches include the maximum entropy<sup>[1b]</sup>, spectral lineshape estimation<sup>[2h]</sup>, tensor structures<sup>[1a]</sup>, compressed sensing (CS)<sup>[2a-f]</sup>, and low-rank<sup>[2g, 2i-l]</sup>. Among them, CS assumes the spectral sparsity of NMR, and utilizes the iterative algorithm to reconstruct spectra. Nevertheless, CS still has some limitations: i) The manual-setting sparseness prior knowledge makes it suboptimal for reconstructing broad peaks<sup>[2g]</sup>; ii) With the decrease of the NUS densities and the increase of the spectra size, the computational time for spectra reconstruction increases significantly. The above issues drive development of new techniques.

Data-driven deep learning (DL) is a hot topic currently. It relies on representative artificial intelligence techniques, neural network<sup>[4]</sup> and massive parallelization with graphic processing units, to greatly reduce the reconstruction time<sup>[3]</sup>. However, there are still many unsolved but important problems in existing DL NMR<sup>[3d]</sup>: i) Too much dependence on training datasets makes

DL lack of robustness and versatility; ii) Too many adjustable parameters make DL require very large pool of training data and consume, an excessively large operative memory; iii) Too complex network architectures make DL hard to be understandable; iv) Limitation on recovering weak peaks make DL difficult to handle high dynamic range spectra, e.g., NOESY; v) To date, an easily-usable DL reconstruction platform for NMR researchers is still not available.

Now, we strongly feel that, so far independent development of optimization and deep learning methods approached to the merging stage, which may inherit the merits of both to breed a stable and high-efficiency strategy in NMR.

Herein, we first devise a model-inspired deep learning framework (MoDern), and then develop a novel cloud computing platform (XCloud-MoDern), to addresses topical challenges presented above (Figure 1).

The complete NMR time-domain signal, called free induction decay (FID), is directly acquire from NMR spectrometers. The forward Fourier transform converts it into an NMR spectrum. In NMR spectroscopy, CS states that the sparsest solution can be always found by the  $l_1$  norm optimization<sup>[2c, 2d, 5]</sup>. This task can be efficiently solved by the Iterative Soft-Thresholding (IST) algorithm<sup>[2c, 2f]</sup>. Initialized with a spectrum with strong artifacts, CS will reconstruct a “clean” spectrum by iteratively alternating data consistency and soft-thresholding.

Once the overall number of iterations is fixed, the data flow can be viewed as our unfolded deep network MoDern (Figure 1B). This architecture provides a rarely available understanding of the complex mapping in deep learning for human NMR experts. Same to CS, the spectrum is forced to maintain the data consistency to the sampled signal. Since the proper choice of thresholds is still of great demand and challenging, thus, instead of manual-setting thresholding in CS, we use a learnable adaptive soft-thresholding module which leverage the frequency characteristics difference across distinct features to adaptively rescale weightings of the network when propagating them through the network, for adaptive soft-thresholding. The key advantage of MoDern is the use of a neural network for defining the optimal threshold for each iteration and for each point in the spectrum. The single learnable adaptive soft-thresholding module is composed of convolutional layers, fully-connected layers, and a soft-thresholding (Figure S1-1). With the increase of iterations, artifacts are gradually removed, and finally a high-quality reconstructed spectrum can be obtained (Supporting Information S1).

[a] Z. Wang, Y. Huang, Y. Zhou, J. Wang, Prof. X. Qu\*  
Department of Electronic Science, Biomedical Intelligent Cloud R&D Center, National Institute for Data Science in Health and Medicine, Xiamen University, P.O.Box 979, Xiamen 361005, China  
\*E-mail: quxiaobo@xmu.edu.cn

[b] Prof. D. Guo, Z. Tu  
School of Computer and Information Engineering, Xiamen University of Technology, Xiamen 361024, China

[c] L. Feng, Prof. D. Lin  
College of Chemistry and Chemical Engineering, Key Laboratory for Chemical Biology of Fujian Province, High-field NMR Center, Xiamen University, Xiamen 361005, China

[d] Y. You  
China Mobile Group, Xiamen 361005, China; Biomedical Intelligent Cloud R&D Center, School of Electronic Science and Engineering (National Model Microelectronics College), Xiamen University, Xiamen 361005, China

[e] Prof. T. Agback  
Department of Molecular Sciences, Swedish University of Agricultural Sciences, Uppsala, Sweden

[f] Prof. V. Orekhov  
Department of Chemistry and Molecular Biology, University of Gothenburg, Box 465, Gothenburg 40530, Sweden

Given the success of training neural networks using solely synthetic data with the exponential functions<sup>[3a, 3c]</sup>, we also employ this scheme to train MoModern to learn the best internal parameters  $\hat{\theta}$  and an optimal mapping  $f(y, \hat{\theta})$  by minimizing the mean square error between outputs of the learnable adaptive soft-thresholding and fully sampled spectra. For a well-trained network, the high-quality spectrum  $\bar{x}$  can be reconstructed reliably and fast from an undersampled signal  $\bar{y}$  via  $f(\bar{y}, \hat{\theta})$ .

Notably, MoModern is inspired by the CS, but go beyond it due to the learning ability and high-efficiency of the deep neural network: i) Different to the self-learning CS often needs lots of iterations, the trained MoModern with the fixed number of iterations is a simple forward model, which greatly shorten the reconstruction time; ii) MoModern produces at least as good spectra reconstruction as CS<sup>[2c]</sup> and often outperforms it for broadest and weakest peaks on both synthetic data and experimental data, which indicate high effective sensitivity<sup>[6]</sup> of MoModern (Supporting Information S4).

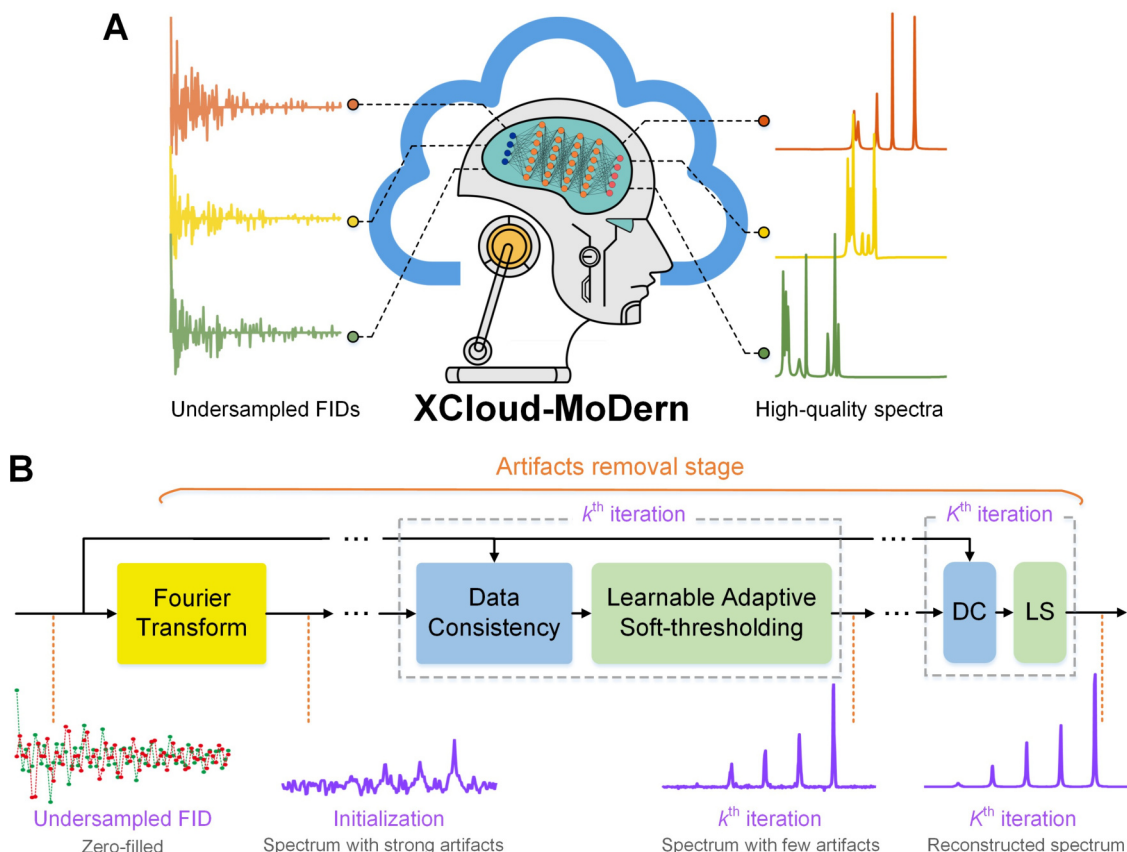


**Figure 1.** An overview of MoModern and XCloud-MoModern. (A) The artificial intelligence cloud computing platform (XCloud-MoModern) for processing multi-dimensional NMR spectra. (B) The recursive MoModern framework that alternates between the data consistency (DC) and the learnable adaptive soft-thresholding (LS). Note:  $k$  ( $k=1, 2, \dots, K$ ) is the number of iterations, a data consistency followed by a learnable adaptive soft-thresholding constitutes an iteration. See Supporting Information S1 for more details.

A key factor that limits wide usage of existing DL for NMR spectra reconstruction is the lack of robustness and versatility. They cannot overcome the common issue of mismatch between training datasets and targets in real applications. It means that NMR researchers need to spend numerous times on re-training networks to handle various reconstruction tasks of different NUS densities, which is obviously unacceptable. MoModern is proposed as a robust and versatile technique that can work effectively in a wide range of scenarios without further training, since introduction of optimization idea endows it a certain degree of stability guaranties. Figure 2A-D show that MoModern maintains the high-quality and significantly better than DLNMR reconstruction performance when the NUS density of spectra significantly deviates from the level used in the training (Supporting Information S5). We want to point out that the

observed phenomenon of MoModern is highly aligned to optimization methods and follows our intuition: The higher NUS densities, the better reconstruction qualities. On the contrary, DLNMR may not improve the reconstruction even with more given sampled points if the mismatch exists.

MoModern costs much less computational time with a lightweight architecture. By abandoning a large number of redundant convolution layers, the number of the network parameters of MoModern is ca 9% of that needed for the state-of-the-art DLNMR<sup>[3a]</sup> (Figure 2E), resulting in a significant reduction in both training and reconstruction time (Figure 2F) without loss of spectral reconstruction quality. Notably, with the increase of the spectra size, the advantage of MoModern in computational time will become more obvious (Supporting Information S7).

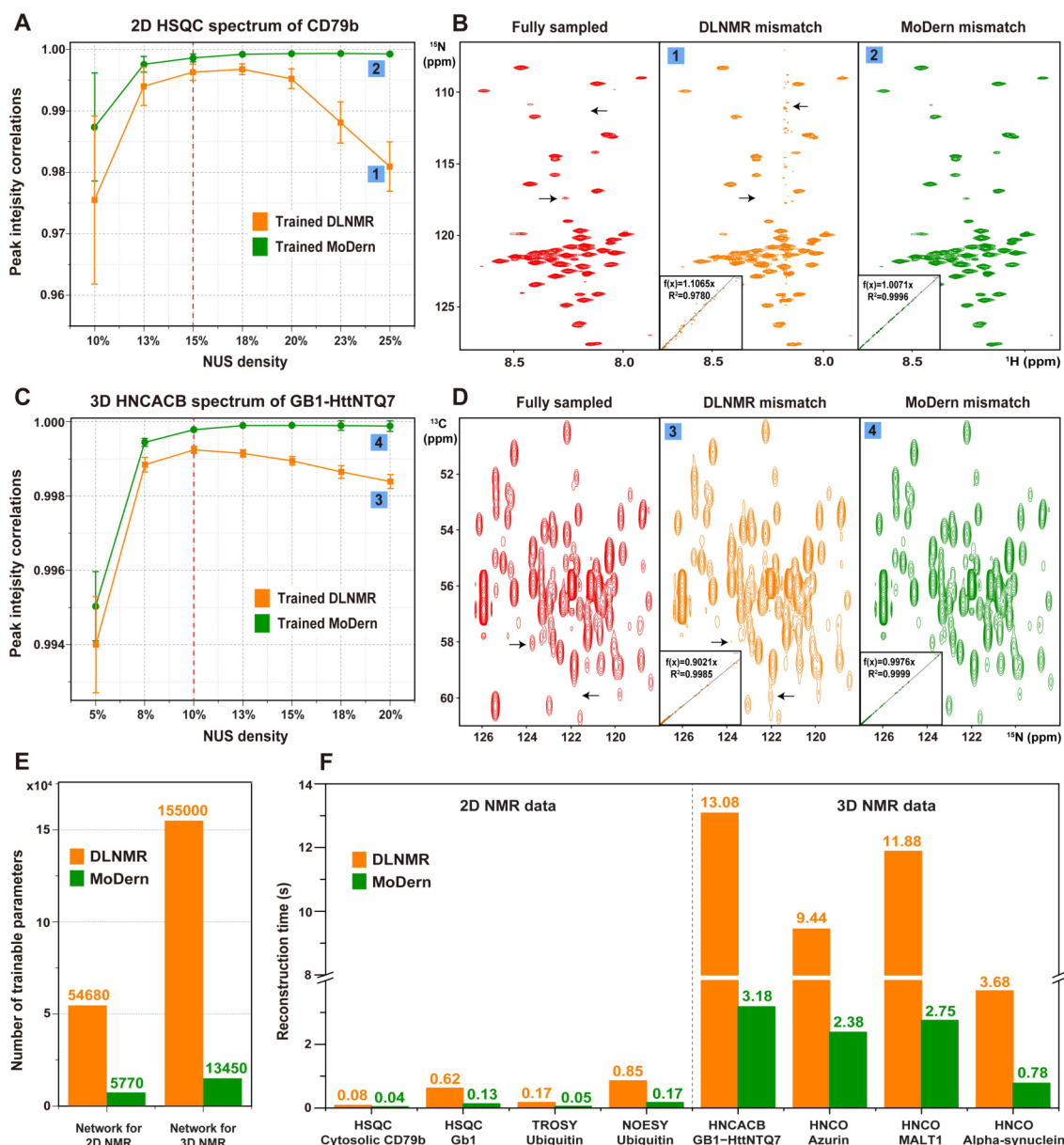


**Figure 2.** Evaluation on robustness and computational time of MoModern. (A) The peak intensity correlations of DLNMR and MoModern trained using 15% NUS density dataset, to reconstruct 2D  $^1\text{H}$ - $^{15}\text{N}$  HSQC spectrum of the cytosolic domain of CD79b, under a series of NUS densities ranging from 10% to 25%. The average and standard deviations of correlations are computed over 100 NUS trials. (B) From the left to right are fully sampled spectrum, the typical of reconstructed results of DLNMR and MoModern trained using 15% NUS density dataset, respectively, to reconstruct spectra from 25% data. (C) The peak intensity correlations of DLNMR and MoModern trained using 10% NUS density dataset, to reconstruct 3D HNCACB spectrum of GB1-HttNTQ7, under a series of NUS densities ranging from 5% to 20%. The average and standard deviations of correlations are computed over 50 NUS trials. (D) From the left to right are fully sampled spectrum, the typical of reconstructed sub-region of the projections on  $^{13}\text{C}$ - $^{15}\text{N}$  planes of DLNMR and MoModern trained using 10% NUS density dataset, respectively, to reconstruct spectra from 20% data. (E) The number of trainable parameters of two networks. (F) The reconstruction time of two networks. Below each bar, the spectrum type, corresponding protein, and spectrum size are listed. For 2D (3D) spectra, the size of the directly detected dimension is followed by the size(s) of the indirect dimension(s). Note: The dashed red line indicates the NUS density that the networks are trained for. The insets of reconstructed spectra show the peak intensity correlation between the fully sampled spectrum and reconstructed spectrum. The  $R^2$  denotes the square of Pearson correlation coefficient. The closer the value of  $R^2$  gets to 1, the stronger the correlation between the fully sampled spectra and the reconstructed spectra is. The obvious intensity distortions and artifacts of DLNMR are marked with the black arrow.

To further demonstrate the reliability and high-quality of MoModern, here, we perform spectrum reconstructions of several challenging cases, including a high dynamic range 2D NOESY spectrum of human Ubiquitin with many weak peaks, a 3D HNCACB spectrum of small protein GB1-HttNTQ7 (10kDa), the 3D HNCACB spectra of a large protein MALT1 (44kDa) and an intrinsically disordered protein Alpha-synuclein (14.5 kDa).

Figure 3A shows that MoModern can faithfully reconstruct the 2D NOESY spectrum using 40% NUS data. We observe 0.9931 correlation (vs the fully sampled spectrum) for the intensities of

the weak peaks (<4% of the highest diagonal peak intensity), which is comparable to CS<sup>[2c]</sup> and greatly outperforms DLNMR<sup>[3a]</sup>. The peak intensity correlations over 0.99 are also observed for three other 2D spectra with moderate dynamic range (Figure S3-1, S3-2, and S3-3).

For ultra-fast high-quality reconstruction of 3D spectra of small, large, and intrinsically disordered proteins, MoModern also shows its great performance. In Figure 3B, for 3D HNCACB spectrum of GB1-HttNTQ7 (10kDa), the peak intensity correlation reaches 0.99 even at 20 times acceleration, i.e., 5% NUS. The excellent

performance also indicates on another 3D HNCQ for Azurin (14kDa), while its peak intensity correlation over 0.99. Figure 3C-D illustrates that, for a large protein MALT1 (44 kDa) and an intrinsically disordered protein Alpha-synuclein (14.5 kDa),

MoDern provides high-quality spectra reconstruction using only 10% NUS data, while DLNMR appears some artifacts (Figure S3-6 and S3-7). Thus, MoDern allows a huge time saving for the experiment of these challenging cases.

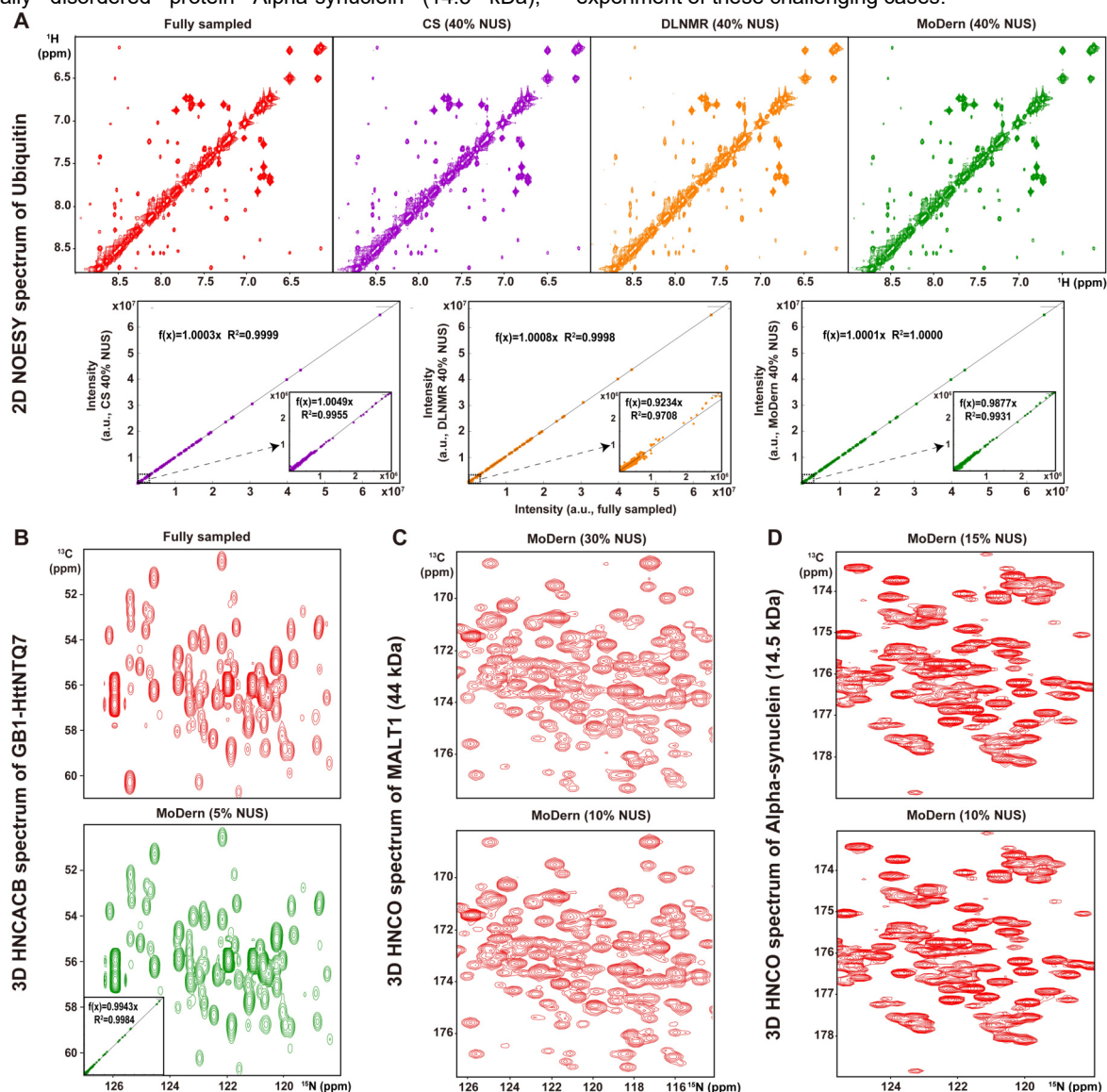


**Figure 3.** The reconstruction performance of MoDern on more challenging cases. (A) 2D  $^1\text{H}$ - $^1\text{H}$  NOESY spectrum reconstruction for human Ubiquitin. The top, from left to right are the fully sampled spectrum, reconstructed spectra using CS, DLNMR, and MoDern from 40% data, respectively. The bottom, from left to right are the peak intensity correlations obtained by CS, DLNMR, and MoDern, respectively. The insets of them are peak intensity correlations of low-intensity peaks ( $<4\%$  of the highest diagonal peak intensity). (B) 3D HNCACB spectrum reconstruction for GB1-HttNTQ7. From top to bottom are the sub-regions of  $^{13}\text{C}$ - $^{15}\text{N}$  projection from the fully sampled spectrum and the reconstructed spectrum using MoDern from 5% data. The inset of reconstructed spectrum shows the peak intensity correlation between fully sampled spectrum and reconstructed spectrum. (C) 3D HNCQ spectrum reconstruction for a large protein MALT1 (44 kDa). From top to bottom are the sub-regions of  $^{13}\text{C}$ - $^{15}\text{N}$  projection from the reconstructed spectra using MoDern from 30% and 10% data, respectively. (D) 3D HNCQ spectrum reconstruction for an intrinsically disordered protein Alpha-synuclein (14.5 kDa). From top to bottom are the sub-regions of  $^{13}\text{C}$ - $^{15}\text{N}$  projection from the reconstructed spectra using MoDern from 15% and 10% data, respectively. Note: The  $R^2$  denotes the square of Pearson correlation coefficient. The experimental data for MALT1 and Alpha-synuclein proteins were acquired under 30% and 15% NUS, respectively. The further retrospectively random undersampling of NUS data is performed to simulate the lower NUS densities.

Quantitative measurement on the relative concentration is analyzed on a mixture of three metabolites, including D-Glucose,  $\beta$ -Alanine and Valine. A time-zero  $^1\text{H}$ - $^{13}\text{C}$  HSQC spectrum ( $\text{HSQC}_0$ ) have better quantitative analysis characteristics that the signal intensities are proportional to concentrations of individual metabolites, and can be obtained by extrapolating a series of 2D  $\text{HSQC}_i$  spectra ( $i = 1, 2, 3$ ) to zero time<sup>[7]</sup> (Supporting Information S6). Figure 4 implies that MoDern provides the closest relative concentration to that of the fully sampled spectrum using 20% NUS data. It demonstrates the reliability of

MoDern, and also makes its large-scale applications become possible.



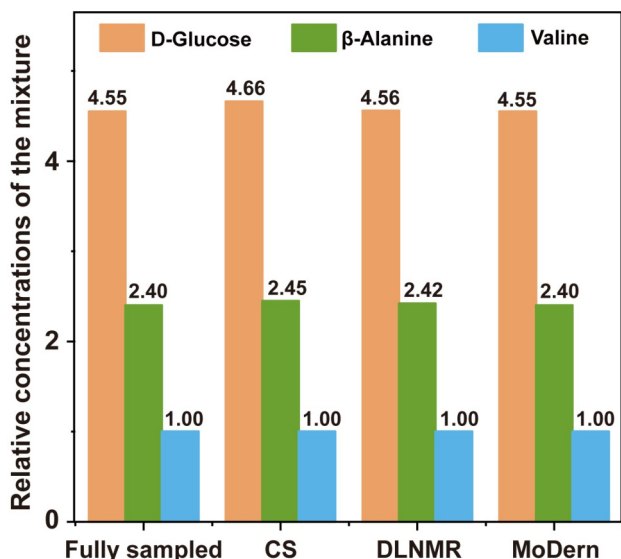


**Figure 4.** Relative concentrations of metabolites in the mixture. From left to right are the fully sampled spectrum, reconstructed results using CS, DLNMR, and MoDern from 20% data, respectively. To improve the concentration of each metabolite, the intensities of multiple, non-overlapping cross peaks assigned to the corresponding metabolite are averaged. The relative concentration of each metabolite is calculated as the volume ratio of a substance to Valine.

Cloud computing platform is generally web-based and easily all-day accessible through a variety of internet-connected devices without installation. Here, to facilitate MoDern's widespread usage in data analysis, we develop XCloud-MoDern, an easy-to-use artificial intelligence cloud computing platform, for easily and fastly processing the NUS multi-dimensional NMR spectra (Figure 5). Up to now, XCloud-MoDern uses MoDern to fast recover high-quality multi-dimensional spectra from NUS data, and also provides a customized retrospectively undersampling technique (NUS simulator). Take reconstruction tasks as the example, the whole workflow is easy and user-friendly to NMR researchers: i) Select the dimensionality (2D or 3D) of the NUS data to be reconstructed; ii) Select the configuration of MoDern; iii) Upload the NUS data file and corresponding NUS mask; iv) Start the reconstruction automatically; v) Download the reconstructed data file and check the reconstruction time. Notably, the waiting time is very short due to the high efficiency of XCloud-MoDern; data is stored in the cloud for reuse and users can also delete it at any time.

Now, XCloud-MoDern is open access to NMR researchers at <http://36.134.147.88:2345/> (Account: CSG-001, Password: CSG@MYTEST\_001). Notably, we decide not to open up the registration in the peer review. We have provided manual, demo data and scripts on the cloud for the quick try. The quality and time of reconstruction on cloud (Table S8-1) is highly consistent with which on local. The screenshots of XCloud-MoDern are shown in Figure S8-1 and S8-2. More information about XCloud-MoDern can be found in Supporting Information S8. We believed that, it will bridge the gap between high-performance and accessible implementations.

Despite the impressive results of current MoDern, it is noteworthy that spectra reconstruction is essentially an ill-posed problem<sup>[3d]</sup>. This indicates that, although DL methods leverage a large amount of well-registered data to learn good transformation, it is theoretically impossible for network inference to realize error-free reconstruction. The distortion still exists on the very low-intensity peaks. Besides, the inadequacy

of training datasets also limits the further improvement of Modern, such as the realization of higher fidelity reconstruction, the application to higher dimensional data (e.g., 4D and 5D) and other experimental types (e.g., diffusion, dynamic, and relaxation).

In summary, we first devise a robust, low-computation-cost, high-fidelity, and ultra-fast deep learning spectra reconstruction approach (MoDern), which breaks through the performance bottleneck of state-of-the-art methods and achieves astonishing performance improvements. Then develop XCloud-MoDern, as a reliable, widely-available, ultra-fast, and easy-to-use artificial intelligence cloud computing platform for highly accelerated NMR. This work is a proof-of-principle demonstration of the effectiveness of merging optimization, deep learning, and cloud computing. We believe that this genre will serve many NMR researchers, and benefit numerous NMR applications in structural and medical biology and may become the mainstream soon.

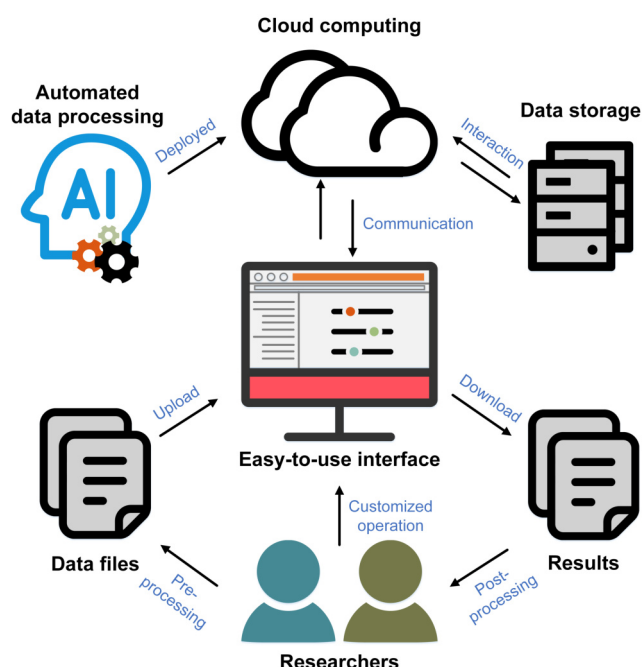


**Figure 5.** XCloud-MoDern now allows researchers to easily and fastly process 2D and 3D NMR data using the deployed methods. The platform has an easy-to-use interface, after uploading the data files and choosing the configuration of methods, the data processing will be automatically carried out in the cloud. Then, users can download the results for further analysis and data is stored in the cloud for reuse.

## Acknowledgements

The authors thank Marius Clore and Samuel Kotler for providing the 3D HNCACB data; Jinfa Ying for assisting in processing and helpful discussions on the 3D HNCACB spectrum; Luke Arbogast and Frank Delaglio for providing the 2D HSQC spectrum of Gb1. The authors thank China Telecom for providing cloud computing service support at initial. The authors also thank NMRPipe and MddNMR for sharing 2D and 3D NMR data on the websites; NMRPipe and SPARKY for data processing support. This work was supported in part by the National Natural Science Foundation of China (NSFC) under grants 61971361, 61871341, and 61811530021, the Joint NSFC-Swedish Foundation for International Cooperation in Research and

Higher Education (STINT) under grant 61811530021, the National Key R&D Program of China under grant 2017YFC0108703, the Natural Science Foundation of Fujian Province of China under grant 2018J06018, the Xiamen University Nanqiang Outstanding Talents Program, the Swedish Research Council under grant 2015-04614, and the Swedish Foundation for Strategic Research under grant ITM17-0218.

## Competing interests

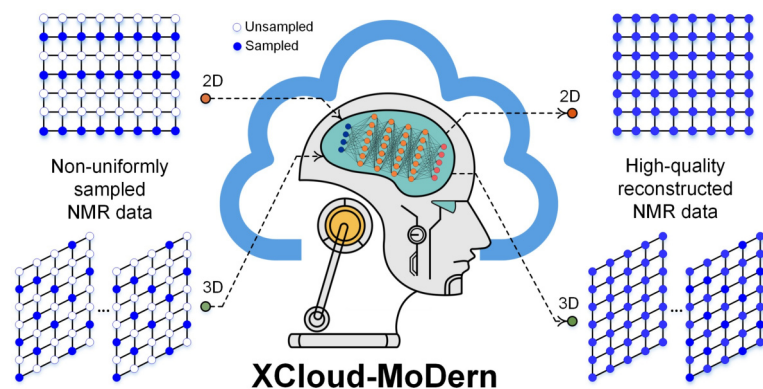
The authors declare no competing interests.

**Keywords:** deep learning • optimization • cloud computing • NMR spectroscopy • fast sampling

- [1] a) V. Jaravine, I. Ibraghimov, V. Yu Orekhov, *Nat. Methods* **2006**, *3*, 605-607; b) M. Mobli, J. C. Hoch, *Prog. Nucl. Magn. Reson. Spectrosc.* **2014**, *83*, 21-41.
- [2] a) X. Qu, X. Cao, D. Guo, Z. Chen, in *International Society for Magnetic Resonance in Medicine 19th Scientific Meeting (ISMRM)*, **2010**, p. 3371; b) X. Qu, D. Guo, X. Cao, S. Cai, Z. Chen, *Sensors* **2011**, *11*, 8888-8909; c) K. Kazimierczuk, V. Y. Orekhov, *Angew. Chem. Int. Ed.* **2011**, *50*, 5556-5559; d) D. J. Holland, M. J. Bostock, L. F. Gladden, D. Nietlispach, *Angew. Chem. Int. Ed.* **2011**, *50*, 6548-6551; e) Y. Shrot, L. Frydman, *J. Magn. Reson.* **2011**, *209*, 352-358; f) S. G. Hyberts, A. G. Milbradt, A. B. Wagner, H. Arthanari, G. Wagner, *J. Biomol. NMR* **2012**, *52*, 315-327; g) X. Qu, M. Mayzel, J.-F. Cai, Z. Chen, V. Orekhov, *Angew. Chem. Int. Ed.* **2015**, *54*, 852-854; h) J. Ying, F. Delaglio, D. A. Torchia, A. Bax, *J. Biomol. NMR* **2017**, *68*, 101-118; i) J. Ying, H. Lu, Q. Wei, J.-F. Cai, D. Guo, J. Wu, Z. Chen, X. Qu, *IEEE Trans. Signal Proces.* **2017**, *65*, 3702-3717; j) J. Ying, J.-F. Cai, D. Guo, G. Tang, Z. Chen, X. Qu, *IEEE Trans. Signal Proces.* **2018**, *66*, 5520-5533; k) H. Lu, X. Zhang, T. Qiu, J. Yang, J. Ying, D. Guo, Z. Chen, X. Qu, *IEEE Trans. Biomed. Eng.* **2018**, *65*, 809-820; l) T. Qiu, Z. Wang, H. Liu, D. Guo, X. Qu, *Magn. Reson. Chem.* **2021**, *59*, 324-345.
- [3] a) X. Qu, Y. Huang, H. Lu, T. Qiu, D. Guo, T. Agback, V. Orekhov, Z. Chen, *Angew. Chem. Int. Ed.* **2020**, *59*, 10297-10300; b) D. F. Hansen, *J. Biomol. NMR* **2019**, *73*, 577-585; c) Y. Huang, J. Zhao, Z. Wang, D. Guo, X. Qu, *arXiv preprint arXiv:2007.06246* **2020**; d) D. Chen, Z. Wang, D. Guo, V. Orekhov, X. Qu, *Chem. -Eur. J.* **2020**, *26*, 10391-10401; e) G. H. Karunanithy, Flemming, *ChemRxiv preprint ChemRxiv:13295888* **2020**.
- [4] Y. LeCun, Y. Bengio, G. Hinton, *Nature* **2015**, *521*, 436-444.
- [5] A. Shchukina, P. Kasprzak, R. Dass, M. Nowakowski, K. Kazimierczuk, *J. Biomol. NMR* **2017**, *68*, 79-98.
- [6] S. G. Hyberts, S. A. Robson, G. Wagner, *J. Biomol. NMR* **2013**, *55*, 167-178.
- [7] K. Hu, W. M. Westler, J. L. Markley, *J. Am. Chem. Soc.* **2011**, *133*, 1662-1665.

---

## Entry for the Table of Contents



The first proof-of-concept of merging optimization, deep learning, and cloud computing, as a reliable, widely-available, ultra-fast, and easy-to-use technique for highly accelerated NMR, and achieves astonishing performance.

---

# Supporting Information

## XCloud-MoDern: An Artificial Intelligence Cloud for Accelerated NMR Spectroscopy

Zi Wang<sup>1</sup>, Di Guo<sup>2</sup>, Zhangren Tu<sup>2</sup>, Yihui Huang<sup>1</sup>, Yirong Zhou<sup>1</sup>, Jian Wang<sup>1</sup>, Liubin Feng<sup>3</sup>, Donghai Lin<sup>3</sup>, Yongfu You<sup>4</sup>, Tatiana Agback<sup>5</sup>, Vladislav Orekhov<sup>6</sup>, Xiaobo Qu<sup>1\*</sup>

<sup>1</sup> Department of Electronic Science, Biomedical Intelligent Cloud R&D Center, National Institute for Data Science in Health and Medicine, Xiamen University, Xiamen 361005, China

<sup>2</sup>School of Computer and Information Engineering, Xiamen University of Technology, Xiamen 361024, China

<sup>3</sup>College of Chemistry and Chemical Engineering, Key Laboratory for Chemical Biology of Fujian Province, High-field NMR Center, Xiamen University, Xiamen 361005, China

<sup>4</sup>China Mobile Group, Xiamen 361005, China; Biomedical Intelligent Cloud R&D Center, School of Electronic Science and Engineering (National Model Microelectronics College), Xiamen University, Xiamen 361005, China

<sup>5</sup>Department of Molecular Sciences, Swedish University of Agricultural Sciences, Uppsala, Sweden

<sup>6</sup>Department of Chemistry and Molecular Biology, University of Gothenburg, Gothenburg 40530, Sweden

\*Correspondence should be addressed to Xiaobo Qu (quxiaobo@xmu.edu.cn)



---

## Supporting Information S1. Methodology

### Generation of the network training and validation datasets

Given the success of training neural networks using solely synthetic data with the exponential functions<sup>[1]</sup>, our network also employs this scheme to form the training dataset and validation dataset, which makes the network training not affected by the lack of realistic data.

In NMR spectroscopy, the typical signal sampled in the time domain  $r$ , called free induction decay (FID), is commonly described as a sum of decaying complex exponents<sup>[2]</sup>:

$$r_n = \sum_{j=1}^J (a_j e^{i\phi_j}) e^{-\frac{n\Delta t}{\tau_j}} e^{in\Delta f_j}, \quad n \in \{1, 2, \dots, N\}, \quad (\text{S1-1})$$

where  $\Delta t$  is the time interval,  $J$  is the number of spectral peaks,  $a_j$ ,  $f_j$ ,  $\tau_j$ , and  $\phi_j$  are the amplitude, frequency, decay time, and phase of the  $j^{\text{th}}$  spectral peak, respectively.

The 40000 fully sampled synthetic FIDs are generated according to Eq. (S1-1) and their parameters are in Table S1-1. The white Gaussian noise at the level with the standard deviation of  $10^{-4}$  is added to each synthetic FID to simulate the realistic NMR data, so that the trained network can be better applied to the reconstruction of measurements.

**Table S1-1. Parameters of the generated synthetic datasets.**

Parameters	Minimum	Increment	Maximum
Number of peaks	1	1	10
Amplitude	0.05	continuous	1.00
Frequency	0.01	continuous	0.99
Decay time	10.00	continuous	179.20
Phase	0	continuous	$2\pi$

Let  $\mathbf{y}$  denotes the FID undersampled by operator  $\mathbf{U}$  following the Poisson-gap sampling scheme<sup>[3]</sup>,  $\mathbf{F}$  denotes the forward Fourier transform, so 40000 undersampled FIDs  $\mathbf{y}=\mathbf{U}\mathbf{r}$  (the sampling mask is different for each of 40000 FIDs to enrich the diversity of the training dataset) and 40000 fully sampled spectra  $\mathbf{x}=\mathbf{F}\mathbf{r}$  are generated correspondingly. To eliminates the dispersion part of the spectrum, make the spectrum “sparser”, and allows spectrum reconstruction with better fidelity and from fewer measurements, virtual echo (VE) method is used<sup>[4]</sup>.

Let  $q=1, 2, \dots, Q$  denotes the  $q^{\text{th}}$  sampling trail, then we have  $Q=40000$  pairs of data  $(\mathbf{y}_q, \mathbf{x}_q)$ . The undersampled FID  $\mathbf{y}_q$  and the fully sampled spectrum  $\mathbf{x}_q$ , are the input and label of the network, respectively. Among the 40000 pairs of data  $(\mathbf{y}_q, \mathbf{x}_q)$ , 90% of the data (36000 pairs) is used as training dataset to train the neural network for obtaining the optimal internal parameters and mapping, and 10% of the data (4000 pairs) is used as validation dataset to adjust the hyper-parameters and evaluate the network’s performance

preliminarily.

The training datasets are shared at the website: <https://github.com/wangziblake/MoDern>.

## The core network structure of MoDern

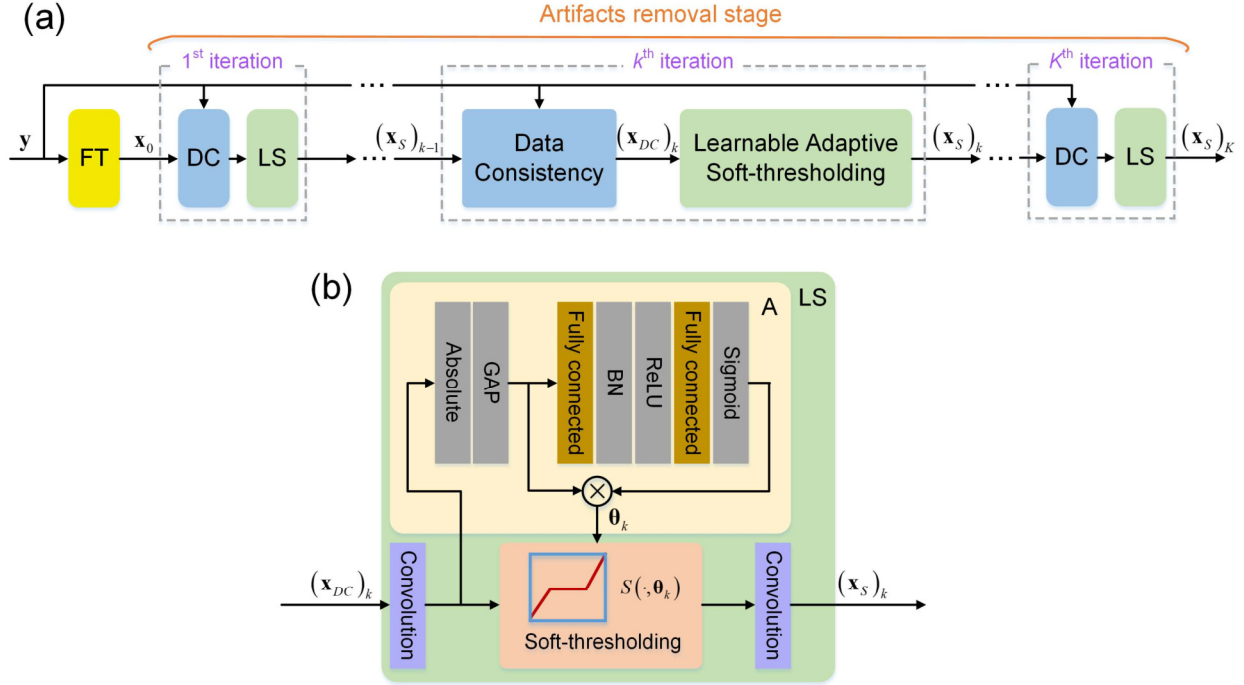


**Figure S1-1.** MoDern: The proposed Model-inspired Deep Learning framework for accelerated NMR spectroscopy. (a) The recursive MoDern framework that alternates between the data consistency (DC), and the learnable adaptive soft-thresholding (LS). (b) The detailed structure of the learnable adaptive soft-thresholding (LS) and threshold auto-setting (A). Note: ‘FT’ is the Fourier transform, ‘GAP’ is the global average pooling, ‘BN’ is the batch normalization, ‘ReLU’ and ‘Sigmoid’ are non-linear functions.

### Data consistency

In this block, each spectrum is forced to maintain the data consistency to the sampled signal, which can ensure reconstructed spectra are aligned to acquired data. Just like the first step of the IST algorithm (Figure S1-1(a)), after inputting the output of the last iteration, i.e., the output of the learnable adaptive soft-thresholding block  $x_S$ , the spectrum becomes

$$\mathbf{x}_{DC} = \mathbf{x}_S + \mathbf{F}\mathbf{U}^T (\mathbf{y} - \mathbf{U}\mathbf{F}^H \mathbf{x}_S), \quad (\text{S1-2})$$

where  $\mathbf{F}$  is the forward Fourier transform, superscript  $H$  denotes the Hermitian conjugate operator,  $\mathbf{x}_{DC}$  is the output of the data consistency block,  $\mathbf{U}$  is the undersampling operator. To show the function of this block more intuitively, Eq. (S1-2) can also be equivalent to

$$(\mathbf{x}_{DC})_n = \begin{cases} \mathbf{x}_S, & n \notin \Omega \\ \mathbf{F}\mathbf{y}, & n \in \Omega \end{cases}, \quad (\text{S1-3})$$

where  $n$  is the index of FIDs and  $\Omega$  is the set of the sampled positions in FIDs. Eq. (S1-3) implies that, at the sampled positions, the points should be replaced with the original inputs  $y$ , while the update of the unsampled points depends entirely on the reconstruction results of the network.

In our implementation, the initial spectrum that inputs the neural network is computed as  $x_0 = FU^T y$ . The initial input  $x_0$  is with strong artifacts since those unsampled FIDs are filled with zeros on non-acquired positions.

### **Learnable adaptive soft-thresholding block**

Soft-thresholding operation is always used to remove irrelevant artifact-related information. In conventional iterative methods [5], the optimal value of the threshold depends on the data, i.e., number of signals and their signal dynamic range, noise level, and even position in the spectrum. Thus, in practice, a relatively safe, high threshold is applied resulting in large number of iterations and, consequently, long calculations as well as poor reconstruction of broad lines. The key advantage of our approach is the use of a neural network for defining the optimal threshold for each iteration and for each point in the spectrum. We introduce the learnable adaptive soft-thresholding, which sets the optimal threshold according to the characteristics of the input, to reduce artifacts of the input spectra. In Figure S1-1(b), the block consists of several elements, including convolution layer, absolute operation, global average pooling (GAP), fully-connected layer, batch normalization (BN), non-linear functions (ReLU and Sigmoid), and soft-thresholding.

Similar to IST algorithm, we directly use the soft-thresholding operation to remove artifacts, and discard a lot of redundant convolution layers[6], which makes the network architecture easier to understand and reduces the computational complexity dramatically. The specific process is as follows: First, we use one convolution layer for the output of the data consistency  $x_{DC}$  to realize feature extraction, then GAP is applied to the absolute values of the feature maps to encode the features of the entire space on each channel as global features  $g$ . After that,  $g$  is fed into a two-layer fully-connected network which contains Sigmoid at the end, so that the excitation values  $\alpha \in (0,1)$  can be obtained. The adaptive selected thresholds are  $\theta = g \cdot \alpha$ . This arrangement is motivated by the fact the threshold not only needs to be positive, but also cannot be too large, thereby preventing the output features from being all zeros. For simplicity, the threshold auto-setting sub-block  $A$  can be regarded as a nonlinear function

$$\theta = A(x_{DC}), \quad (S1-4)$$

The adaptive-setting thresholds  $\theta$  are used in the soft-thresholding operation  $S$ . Note that, an individual threshold is applied to each channel of the feature map. Finally, we can obtain the output spectrum  $x_s$  through one convolution layer, which restores the number of channels of the feature map to be consistent with  $x_{DC}$ . The overall learnable adaptive soft-thresholding  $LS$  is

$$x_s = LS(x_{DC}, \theta). \quad (S1-5)$$

In our implementation, the architecture-related hyper-parameters of the network are listed in Table S1-2.

The learnable adaptive soft-thresholding are interleaved with data consistency, to remove artifacts gradually, and finally the high-quality reconstructed spectra can be obtained.

**Table S1-2.** Architecture-related hyper-parameters of the learnable adaptive soft-thresholding. ‘Conv’ is the convolution layer, ‘FC’ is the fully-connected layer. Take 2D NMR for example, 1, N, 2 in the output size ‘1×N×2’ represent the number of width, height, and channels of the feature map, respectively. 1, 3, 2, 32 in the hyper-parameters of Conv ‘1×3×2, 32’ represent the size and the number of filters. 32 in the hyper-parameters of FC ‘32’ represent the number of neurons.

Operations	2D NMR		3D NMR	
	Hyper-parameters	Output size	Hyper-parameters	Output size
Input	/	1×N×2	/	1×(N <sub>1</sub> ×N <sub>2</sub> )×2
1 <sup>st</sup> Conv	1×3×2, 32	1×N×32	3×3×2, 32	1×(N <sub>1</sub> ×N <sub>2</sub> )×32
1 <sup>st</sup> FC	2	1×1×2	2	1×(1×1)×2
2 <sup>nd</sup> FC	32	1×1×32	32	1×(1×1)×32
2 <sup>nd</sup> Conv (output)	1×3×32, 2	1×N×2	3×3×32, 2	1×(N <sub>1</sub> ×N <sub>2</sub> )×2

## Loss function and implementation details

In the training stage, let  $k$  represents the  $k^{th}$  iteration, and  $\Theta$  denotes the network trainable parameters, then the output at the  $k^{th}$  phase is  $\hat{\mathbf{x}}_k(\Theta, \mathbf{y})$ , and the total number of iterations is  $K$ . The overall loss function is

$$L(\Theta) = \frac{1}{KQ} \sum_{k=1}^K \sum_{q=1}^Q \left\| \mathbf{x}_{ref} - \hat{\mathbf{x}}_k^q(\Theta, \mathbf{y}) \right\|_2^2, \quad (\text{S1-6})$$

where  $q$  is the  $q^{th}$  ( $q=1, 2, \dots, Q$ ) FID signals, and  $\mathbf{x}_{ref}$  is the label spectrum. The number of iterations of MoDern are 10, i.e.,  $K=10$ . He initialization<sup>[7]</sup> is used to initialize the network weights, Adam<sup>[8]</sup> is selected as the optimizer. The batch size is 10. The initial learning rate was set to 0.001 with an exponential decay of 0.95. Thus, the optimal parameters  $\hat{\Theta}$  are obtained by minimizing the loss function on the training dataset. The total training time are 3.9 hours and 15.1 hours for 2D and 3D NMR within 80 epochs, respectively. We use the relative  $l_2$  norm error  $RLNE = \frac{\|\mathbf{x}_{ref} - \hat{\mathbf{x}}\|_2}{\|\mathbf{x}_{ref}\|_2}$  as the quantitative criteria to evaluate the reconstruction performances in the training stage, where  $\mathbf{x}_{ref}$  is the fully sampled spectrum and  $\hat{\mathbf{x}}$  is the reconstructed spectrum. Note that, the lower  $RLNE$  represents the better performance. Figure S1-2 shows that MoDern has good convergence on both training datasets and validation datasets.

In the reconstruction stage, for given undersampled FID signals  $\bar{\mathbf{y}}$  which needs to be reconstructed, we can get the reconstructed result  $\bar{\mathbf{x}} = f(\bar{\mathbf{y}}, \hat{\Theta})$  through the trained network, where  $\hat{\Theta}$  and  $f(\mathbf{y}, \hat{\Theta})$  are optimal network parameters and the optimal mapping, respectively. Notably, MoDern is very flexible and robust, the network which is trained once under a given NUS density and spectra dimensionality (2D or 3D) can be directly applied to reconstruct the spectra with different sizes and types on different NUS density, and maintain the stable performance. So that, re-training of the network is not needed for different spectra provided that the datasets have the same dimensionality (Supporting Information S4).



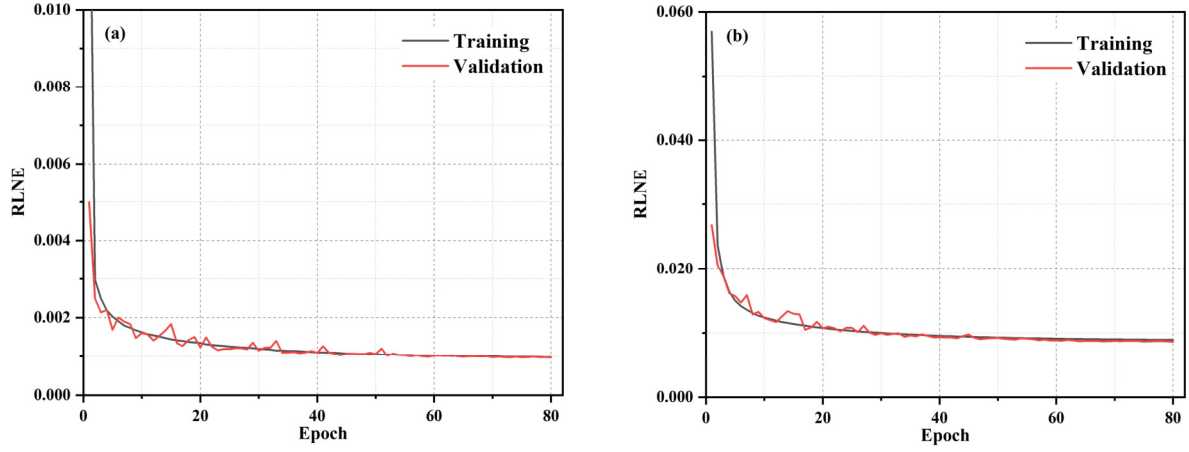


**Figure S1-2.** Good convergence of MoDern on both training datasets and validation datasets. The training and validation *RLNE* curves of MoDern for (a) 2D NMR with 20% NUS, (b) 3D NMR with 10% NUS.

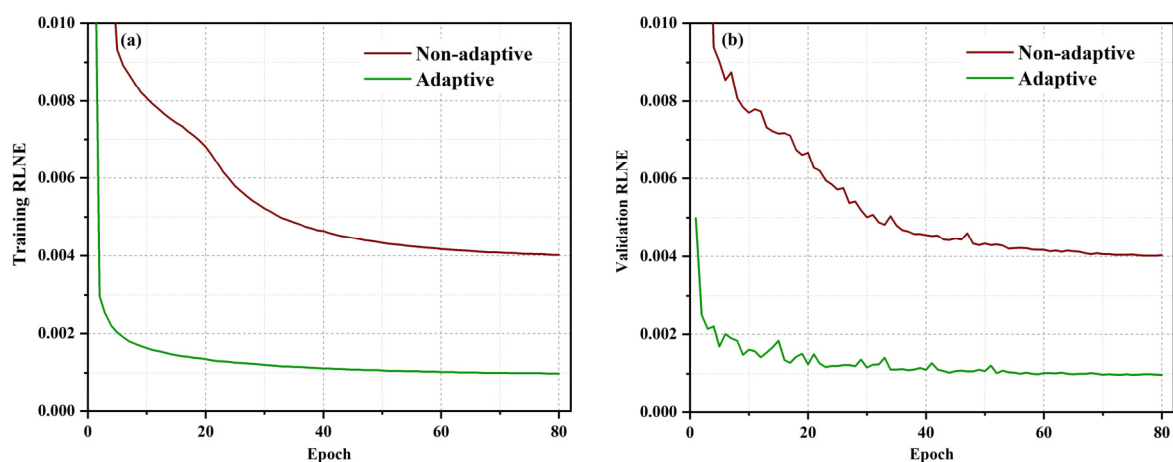
## Discussion on the adaptive soft-thresholding

Threshold plays an important role in the reconstruction results and exploring the proper choice of it is still of great demand and challenging. For a deep neural network with the fixed number of iterations, a too small threshold makes the majority of the artifacts remains since the effect of the  $l_1$  norm minimization is ignorable; a too large one results in serious distortion of the reconstructed spectra.

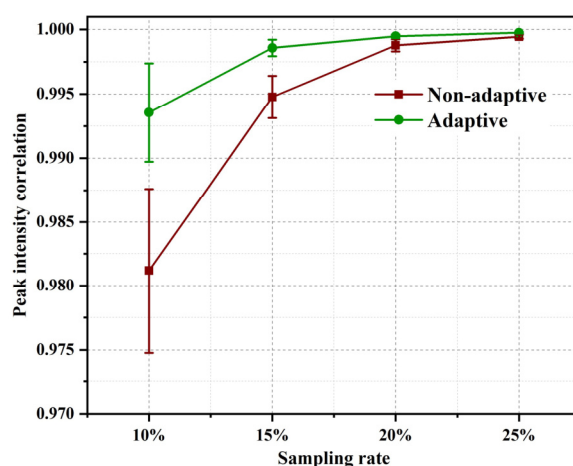
Herein, we discuss the necessity of employing adaptive soft-thresholding by comparing reconstruction results of networks with and without adaptability. The adaptive network is the proposed MoDern. The non-adaptive network is to remove the threshold auto-setting sub-block  $A$ , so that thresholds in a trained network are fixed and should not change with the characteristics of the input.

Figure S1-3 shows that, in the training stage, the adaptive network MoDern has lower reconstruction error and faster convergence speed on both training datasets and validation datasets, which implies its higher reconstruction fidelity. The above viewpoint is confirmed by the realistic NMR data. In Figure S1-4, the adaptive network MoDern surpasses the non-adaptive network in spectra quality, while being robust and can maintain excellent performance at low NUS density.

Therefore, the adaptive soft-thresholding scheme is used to achieve more excellent and robust reconstruction results of NMR spectra.



**Figure S1-3.** The *RLNE* curve of training datasets and validation datasets in the network training stage for 2D NMR. (a) The *RLNE* curve of training datasets of two network strategies. (b) The *RLNE* curve of validation datasets of two network strategies. Note: The proposed MoDern uses the ‘adaptive soft-thresholding’ strategy, due to its lowest *RLNE* on both two datasets.



**Figure S1-4.** Peak intensity correlation obtained by the network with/without adaptive soft-thresholding under different NUS levels for 2D HSQC spectrum of cytosolic CD79b. Note: The  $R^2$  denotes the square of Pearson correlation coefficient. The average and standard deviations of correlations are computed over 100 NUS trials. The closer the value of  $R^2$  gets to 1, the stronger the correlation between the fully sampled spectra and the reconstructed spectra is.

## Supporting Information S2. Experimental setups of the NMR spectra

The important information on the NMR spectra used for reconstruction, including five 2D spectra and four 3D spectra of small, large and intrinsically disordered proteins, are listed in Table S2-1. More details on experimental setup could be found below. The direct dimension of all spectra was processed in NMRPipe<sup>[9]</sup> before performing reconstructions.

**Table S2-1.** Information on the NMR spectra used for reconstruction. For 2D (3D) spectra, the size of the directly detected dimension is followed by the size(s) of the indirect dimension(s). The NUS means that the FID data were acquired on spectrometer in non-uniform sampling mode for reducing data acquisition time.

Spectra Type		Samples	Molecular weight	Spectra size for reconstruction	Sampling type
2D	NOESY	Ubiquitin	7 kDa	928 × 512	Full
	HSQC	CD79b	5.7 kDa	116 × 256	Full
	HSQC	Gbl	8.0 kDa	1146 × 170	Full
	TROSY	Ubiquitin	8.6 kDa	512 × 128	Full
	HSQC	Mixture	/	1024 × 256	Full
3D	HNCACB	GB1-HttNTQ7	10 kDa	879 × 90 × 44	Full
	HNCO	Azurin	14 kDa	732 × 60 × 60	Full
	HNCO	MALT1	44 kDa	735 × 57 × 70	30% NUS
	HNCO	Alpha-synuclein	14.5 kDa	221 × 64 × 64	15% NUS

### 2D spectra

The 2D <sup>1</sup>H-<sup>1</sup>H NOESY spectrum of human ubiquitin was acquired from ubiquitin at 298K on an 600 MHz Varian spectrometer as was described previously<sup>[5a]</sup>. The fully sampled spectrum has 928 × 512 complex points, the size of the directly detected dimension (<sup>1</sup>H) is followed by the size of the indirect dimension (<sup>1</sup>H).

The 2D <sup>1</sup>H-<sup>15</sup>N HSQC spectrum of cytosolic CD79b protein was acquired for 300 μM <sup>15</sup>N-<sup>13</sup>C labeled sample of cytosolic CD79b in 20 mM sodium phosphate buffer at 298K on an 800 MHz Bruker spectrometer as was described previously<sup>[1, 2b]</sup>. The fully sampled spectrum has 1024 × 256 complex points, the size of the directly detected dimension (<sup>1</sup>H) is followed by the size of the indirect dimension (<sup>15</sup>N).

The 2D <sup>1</sup>H-<sup>15</sup>N HSQC spectrum of Gbl was acquired from GB1 at 298K on a 600 MHz Bruker spectrometer as was described previously<sup>[1]</sup>. The fully sampled spectrum has 1676 × 170 complex points, the size of the directly detected dimension (<sup>1</sup>H) is followed by the size of the indirect dimension (<sup>15</sup>N).

The 2D <sup>1</sup>H-<sup>15</sup>N TROSY spectrum of ubiquitin was acquired from ubiquitin at 298K on an 800 MHz Bruker spectrometer as was described previously<sup>[4]</sup>. The fully sampled spectrum has 682 × 128 complex points, the

---

size of the directly detected dimension ( $^1\text{H}$ ) is followed by the size of the indirect dimension ( $^{15}\text{N}$ ).

The 2D  $^1\text{H}$ - $^{13}\text{C}$  HSQC spectrum of a mixture of three metabolites, including 24.27 mM D-Glucose, 11.49 mM  $\beta$ -Alanine, 5.38 mM D-Mannose and dissolved in 0.5ml  $\text{D}_2\text{O}$ . It was acquired using a phase sequence (hsqcct2etgp2sq.2.khu) at 298 K on a Bruker Avance III-HD 850 MHz spectrometer using 5mm CPTCI probe. The fully sampled spectrum has  $1024 \times 256$  complex points, the size of the directly detected dimension ( $^1\text{H}$ ) is followed by the size of the indirect dimension ( $^{13}\text{C}$ ).

### 3D spectra

The fully sampled 3D HNCACB spectrum of GB1-HttNTQ7 was acquired at 298K on a 700 MHz Bruker spectrometer as was described previously<sup>[10]</sup>. The fully sampled spectrum has  $1024 \times 90 \times 44$  complex points, the size of the directly detected dimensions ( $^1\text{H}$ ) is followed by the size of the indirect dimensions ( $^{15}\text{N}$  and  $^{13}\text{C}$ ).

The fully sampled 3D HNCO spectrum of Azurin protein was acquired on an 800 MHz Bruker spectrometer as was described previously<sup>[11]</sup>. The fully sampled spectrum has  $1024 \times 60 \times 60$  complex points, the size of the directly detected dimensions ( $^1\text{H}$ ) is followed by the size of the indirect dimensions ( $^{15}\text{N}$  and  $^{13}\text{C}$ ).

The NUS 3D HNCO spectrum of MALT1 protein was acquired at 298K on a 700 MHz Bruker spectrometer as was described previously<sup>[11]</sup>. Only 30% NUS data were recorded in the experiment. The expected fully spectrum has  $1024 \times 57 \times 70$  complex points, the size of the directly detected dimensions ( $^1\text{H}$ ) is followed by the size of the indirect dimensions ( $^{15}\text{N}$  and  $^{13}\text{C}$ ).

The NUS 3D HNCO spectrum of Alpha-synuclein protein was acquired at 293K on an 800 MHz Bruker spectrometer as was described previously<sup>[12]</sup>. Only 15% NUS data were recorded in the experiment. The expected fully spectrum has  $1024 \times 64 \times 64$  complex points, the size of the directly detected dimensions ( $^1\text{H}$ ) is followed by the size of the indirect dimensions ( $^{15}\text{N}$  and  $^{13}\text{C}$ ).



---

## Supporting Information S3. More details on spectra reconstruction

The proposed MoDern will be compared with two state-of-the-art NMR spectra reconstruction methods, including a model-based optimization method (CS<sup>[5a]</sup>) and a data-driven deep learning method (DLNMR<sup>[1]</sup>). And all undersampled spectra are generated according to Poisson-gap sampling<sup>[3]</sup>. Notably, for the same spectra dimensionality (2D or 3D) and NUS density, all reconstruction results are obtained by the same MoDern network, without re-training.

### Reconstruction of 2D spectra

Fully sampled data were acquired for all 2D spectra. The existence of fully sampled spectra would be helpful serving as the golden standard in reconstruction validation. The undersampled FID were obtained by retrospectively undersampling the fully sampled FID.

To demonstrate the applicability of the trained MoDern in 2D spectra, we reconstruct four spectra, including the 2D <sup>1</sup>H-<sup>1</sup>H NOESY spectrum of human ubiquitin (Main text Figure 3A), the 2D <sup>1</sup>H-<sup>15</sup>N HSQC spectrum of CD79b (Figure S3-1), the 2D <sup>1</sup>H-<sup>15</sup>N HSQC spectrum of Gb1 (Figure S3-2), and the 2D <sup>1</sup>H-<sup>15</sup>N TROSY spectrum of ubiquitin (Figure S3-3).

For the reconstruction of a high dynamic range NOESY spectrum with many weak peaks at the NUS density of 40% (Main text Figure 3A), MoDern and CS also can obtain high correlations ( $>0.99$ ) even on low-intensity peaks, while DLNMR fails to handle this scenario.

For the reconstruction of three spectra with moderate dynamic range at the NUS density of 20% (Figure S3-1, S3-2, S3-3), MoDern can obtain very high peak intensity correlation ( $>0.99$ ), and representative lineshapes of the spectra closing to the fully sampled spectra can demonstrate this. CS and DLNMR also can achieve high peak intensity correlation,  $>0.98$  and  $>0.97$ , respectively.

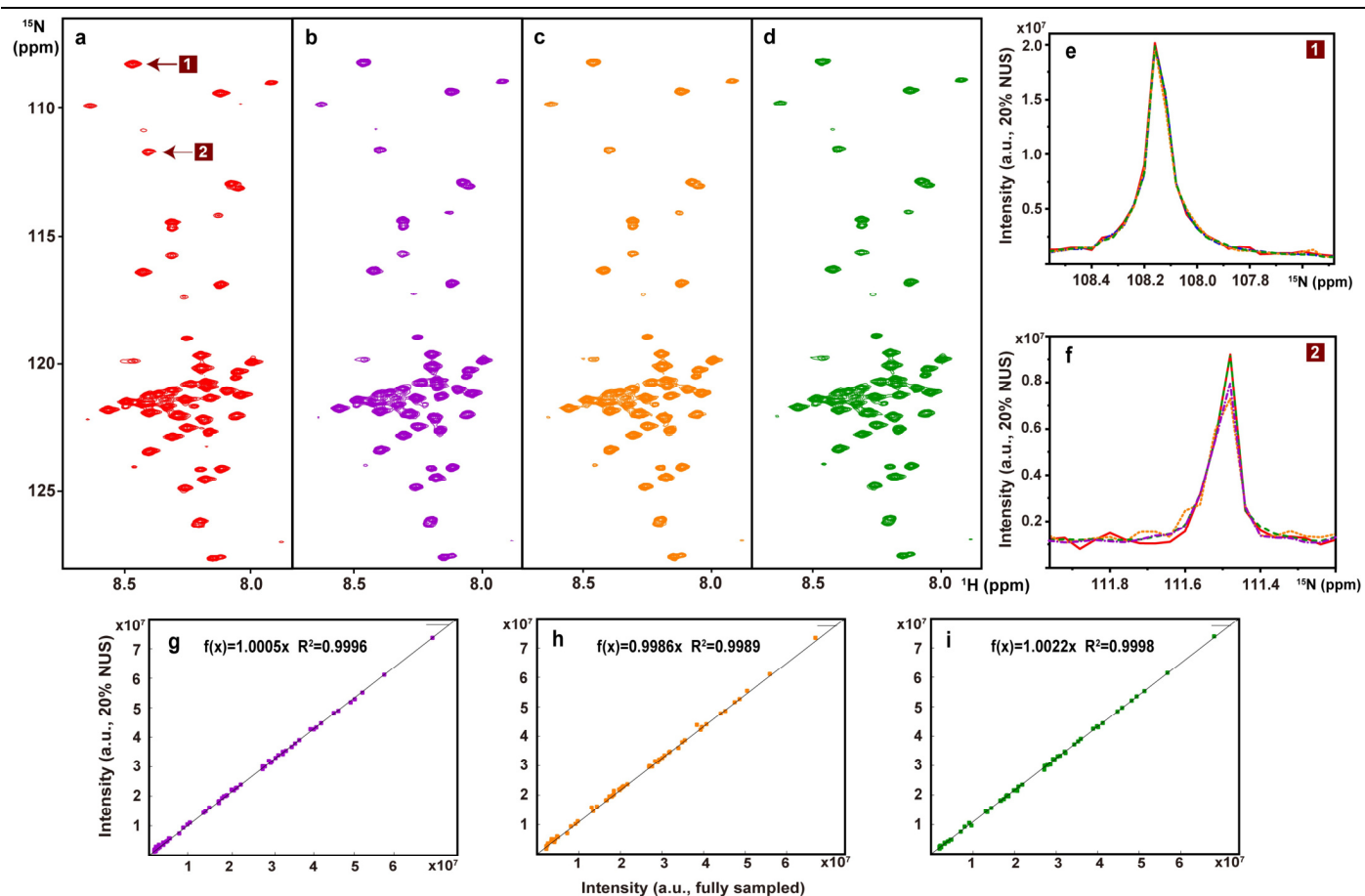


**Figure S3-1.** 2D  $^1\text{H}$ - $^{15}\text{N}$  HSQC spectrum of the cytosolic domain of CD79b protein from the B-cell receptor. (a) The fully sampled spectrum. (b), (c) and (d) are reconstructed spectra using CS, DLNMR, and MoDern from 20% data, respectively. (e) and (f) are zoomed out 1D  $^{15}\text{N}$  traces, and the red, purple, orange, and green lines represent the fully sampled spectra, CS, DLNMR, and MoDern reconstructed spectra, respectively. (g), (h), and (i) are the peak intensity correlations obtained by CS, DLNMR, and MoDern, respectively.

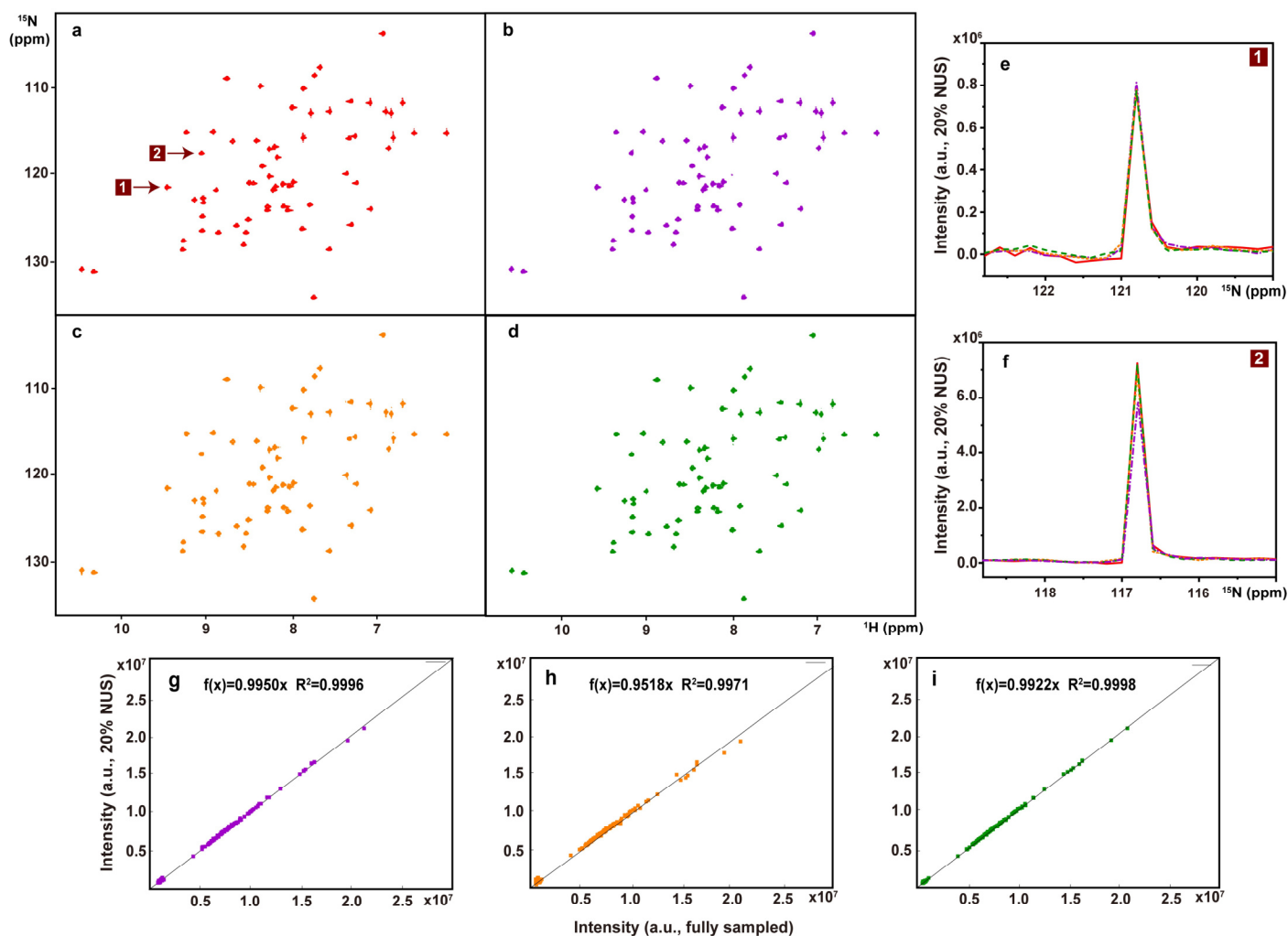


**Figure S3-2.** 2D  $^1\text{H}$ - $^{15}\text{N}$  HSQC spectrum of Gb1. (a) The fully sampled spectrum. (b), (c) and (d) are reconstructed spectra using CS, DLNMR, and MoDern from 20% data, respectively. (e) and (f) are zoomed out 1D  $^{15}\text{N}$  traces, and the red, purple, orange, and green lines represent the fully sampled spectra, CS, DLNMR, and MoDern reconstructed spectra, respectively. (g), (h), and (i) are the peak intensity correlations obtained by CS, DLNMR, and MoDern, respectively.

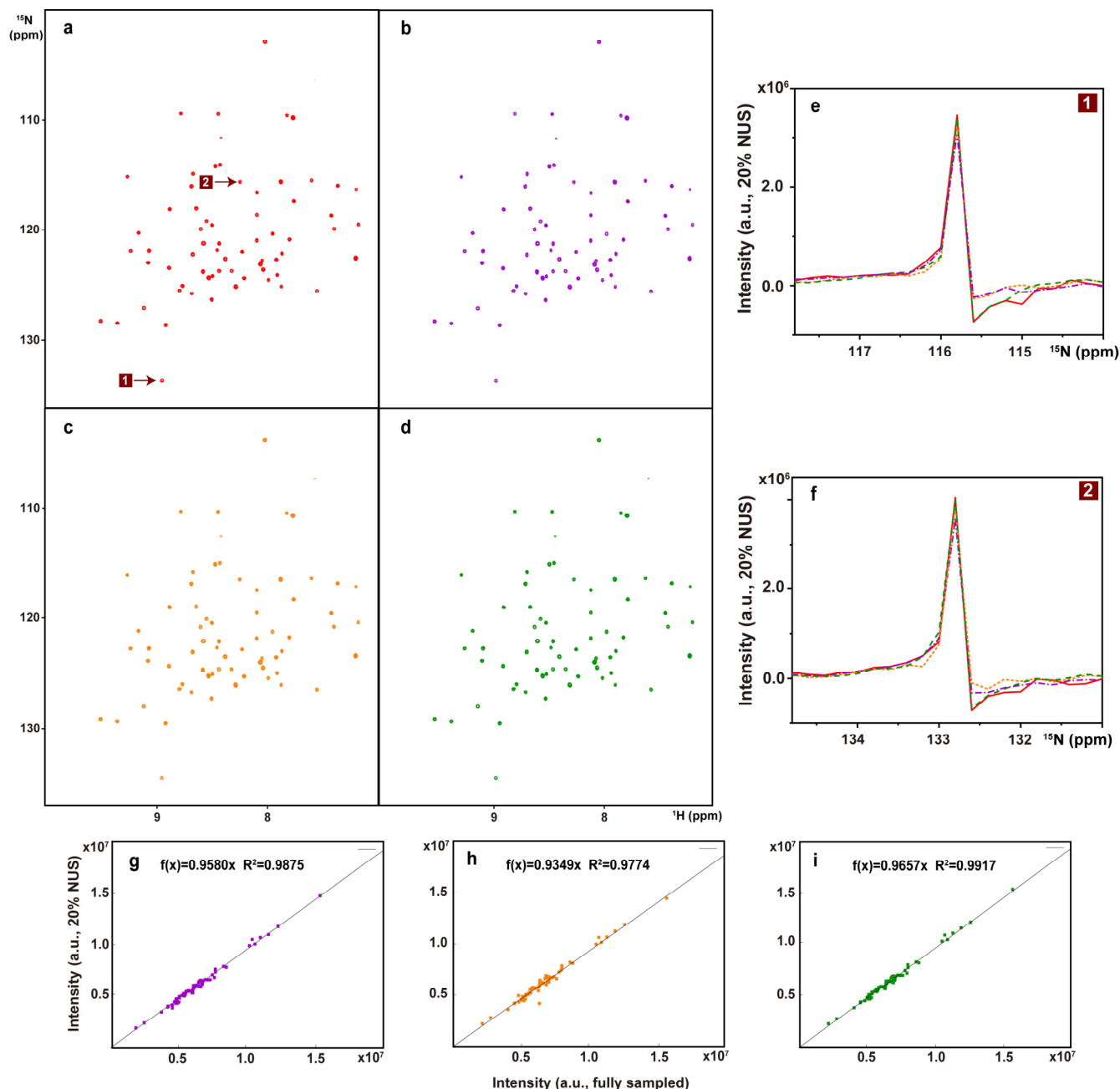


**Figure S3-3.** 2D  $^1\text{H}$ - $^{15}\text{N}$  TROSY spectrum of ubiquitin. (a) The fully sampled spectrum. (b), (c) and (d) are reconstructed spectra using CS, DLNMR, and MoDern from 20% data, respectively. (e) and (f) are zoomed out 1D  $^{15}\text{N}$  traces, and the red, purple, orange, and green lines represent the fully sampled spectra, CS, DLNMR, and MoDern reconstructed spectra, respectively. (g), (h), and (i) are the peak intensity correlations obtained by CS, DLNMR, and MoDern, respectively.

## Reconstruction of 3D spectra

To demonstrate the applicability of the trained MoDern in 3D spectra, we reconstruct four spectra of small, large and intrinsically disordered proteins, including the 3D HNCACB spectrum of GB1-HttNTQ7 (Main text Figure 3B and Figure S3-4), the 3D HNCO spectrum of Azurin protein (Figure S3-5), the 3D HNCO spectrum of MALT1 protein (Main text Figure 3C and Figure S3-6), and the 3D HNCO spectrum of Alpha-synuclein



protein (Main text Figure 3D and Figure S3-7).

### Reconstruction of 3D spectra of small proteins

Fully sampled FID data were acquired for two small proteins, including the GB1-HttNTQ7 and Azurin. The existence of fully sampled spectra would be helpful serving as the golden standard in reconstruction validation. The undersampled FID were obtained by retrospectively undersampling the fully sampled FID.

For the reconstruction of two spectra of small proteins (Figure S3-4 and S3-5), all of three methods CS, DLNMR, and MoDern can produces nice reconstructions that are very closing to the fully sampled ones. And the peak intensity correlations of them with  $R^2 > 0.99$  shows the high fidelity of reconstruction.

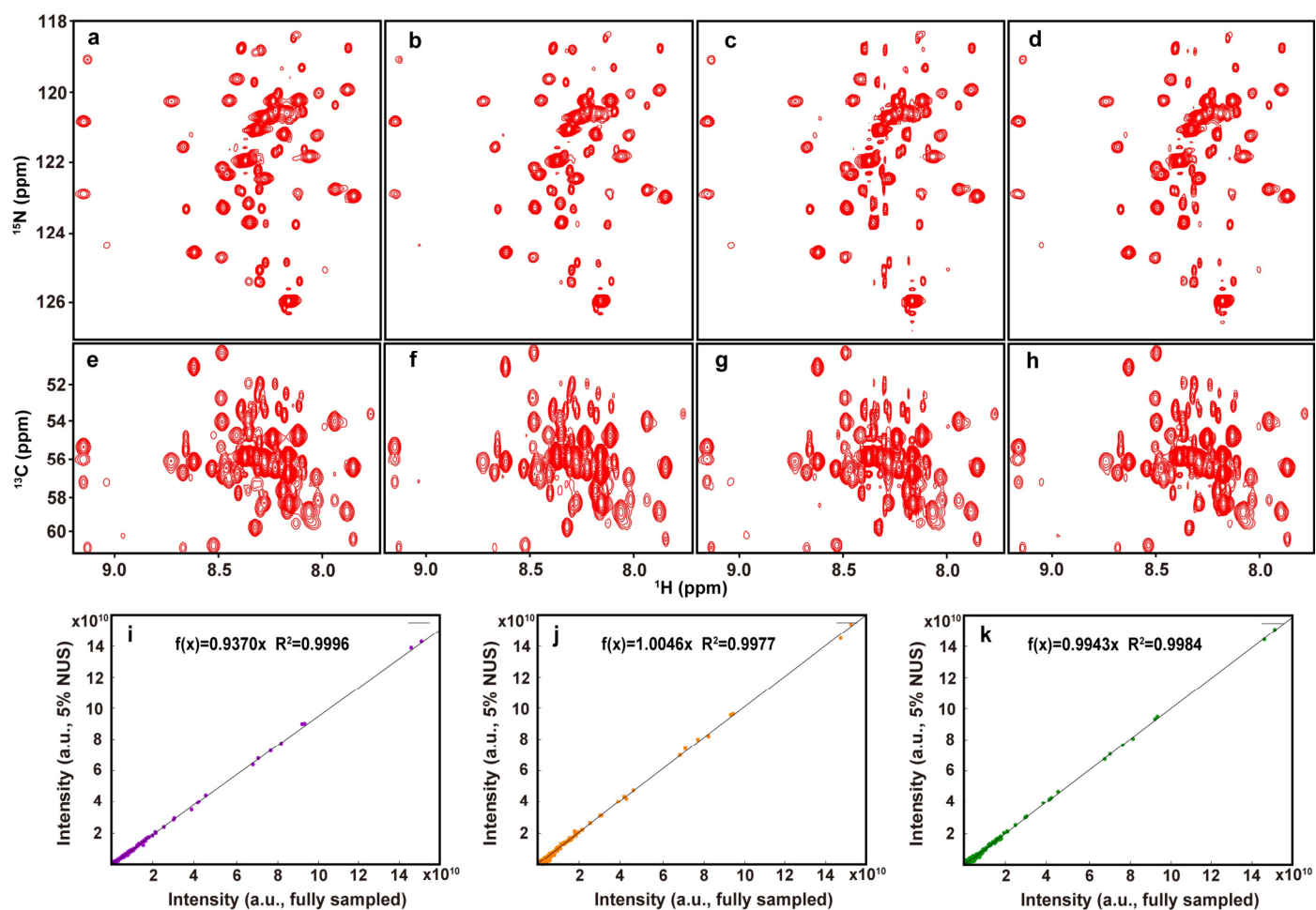


**Figure S3-4.** The sub-region of the projections on  $^1\text{H}$ - $^{15}\text{N}$  and  $^1\text{H}$ - $^{13}\text{C}$  planes of the 3D HNCACB spectrum of GB1-HttNTQ7. (a) and (e) are projections of the fully sampled spectrum. (b) and (f) are projections of the CS reconstructed spectrum. (c) and (g) are projections of the DLNMR reconstructed spectrum. (d) and (h) are projections of the MoDern reconstructed spectrum. (i), (j), and (k) are the peak intensity correlations obtained by CS, DLNMR, and MoDern, respectively. Note: 5% NUS data were acquired for reconstruction.

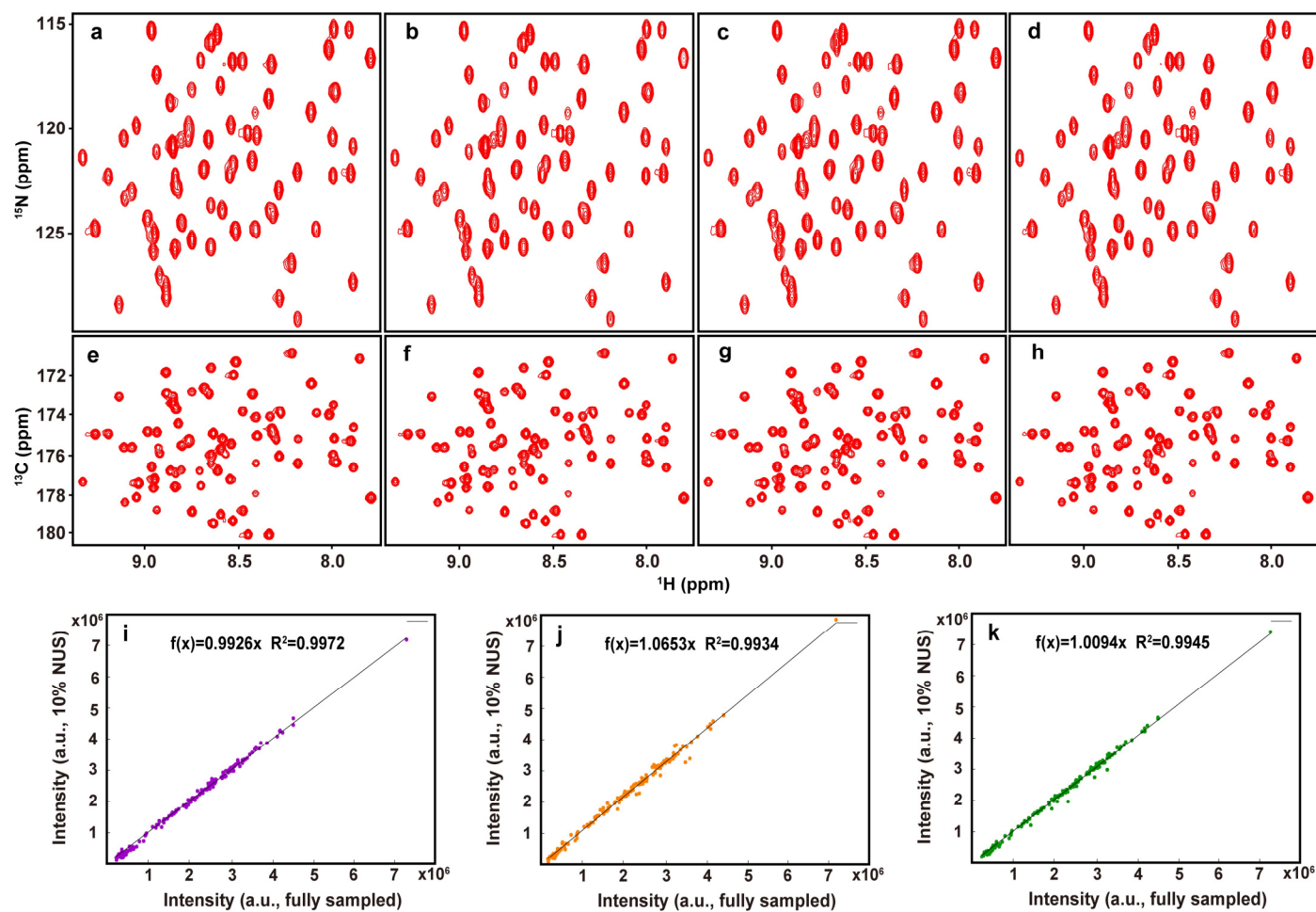


**Figure S3-5.** The sub-region of the projections on  $^1\text{H}$ - $^{15}\text{N}$  and  $^1\text{H}$ - $^{13}\text{C}$  planes of the 3D HNCO spectrum of Azurin protein. (a) and (e) are projections of the fully sampled spectrum. (b) and (f) are projections of the CS reconstructed spectrum. (c) and (g) are projections of the DLNMR reconstructed spectrum. (d) and (h) are projections of the MoDern reconstructed spectrum. (i), (j), and (k) are the peak intensity correlations obtained by CS, DLNMR, and MoDern, respectively. Note: 10% NUS data were acquired for reconstruction.

### Reconstruction of 3D spectra of a large protein and an intrinsically disordered protein

Partial FID data were acquired for a large protein (MALT1, 44 kDa) and an intrinsically disordered protein (Alpha-synuclein, 14.5 kDa). These two spectra were experimentally recorded with non-uniform sampling technique in spectrometers for reducing data acquisition time.

For the large protein, i.e., MALT1, the reconstructed spectra were depicted in Figure S3-6. Results show that all of three methods CS, DLNMR, and MoDern can reconstruct the HNCO spectra very well with 30% NUS data, implying that 30% data would be adequate for reconstruction methods to provide reliable results. Here, we performed retrospectively undersampling on the 30% NUS data, taking one out the three data points randomly for emulating the 10% NUS in experiments. The reconstructed spectra by MoDern from 10% NUS data are very similar to the spectra reconstructed using 30% NUS data and the reconstruction performance on relatively weak peaks is better than CS and DLNMR, indicating that MoDern still offers nice reconstruction

even under the high acceleration factor.

For an intrinsically disordered protein, i.e., Alpha-synuclein, the reconstructed spectra were shown in Figure S3-7. Results show that all of three methods CS, DLNMR, and MoDern can give nice reconstructions with 15% NUS data. Here, we performed retrospectively undersampling on the 15% NUS data, taking two out the three data points randomly for emulating the 10% NUS in experiments. Even under a higher acceleration, only 10% data used for reconstruction, both MoDern and CS still allow good reconstruction, while DLNMR appears some artifacts.

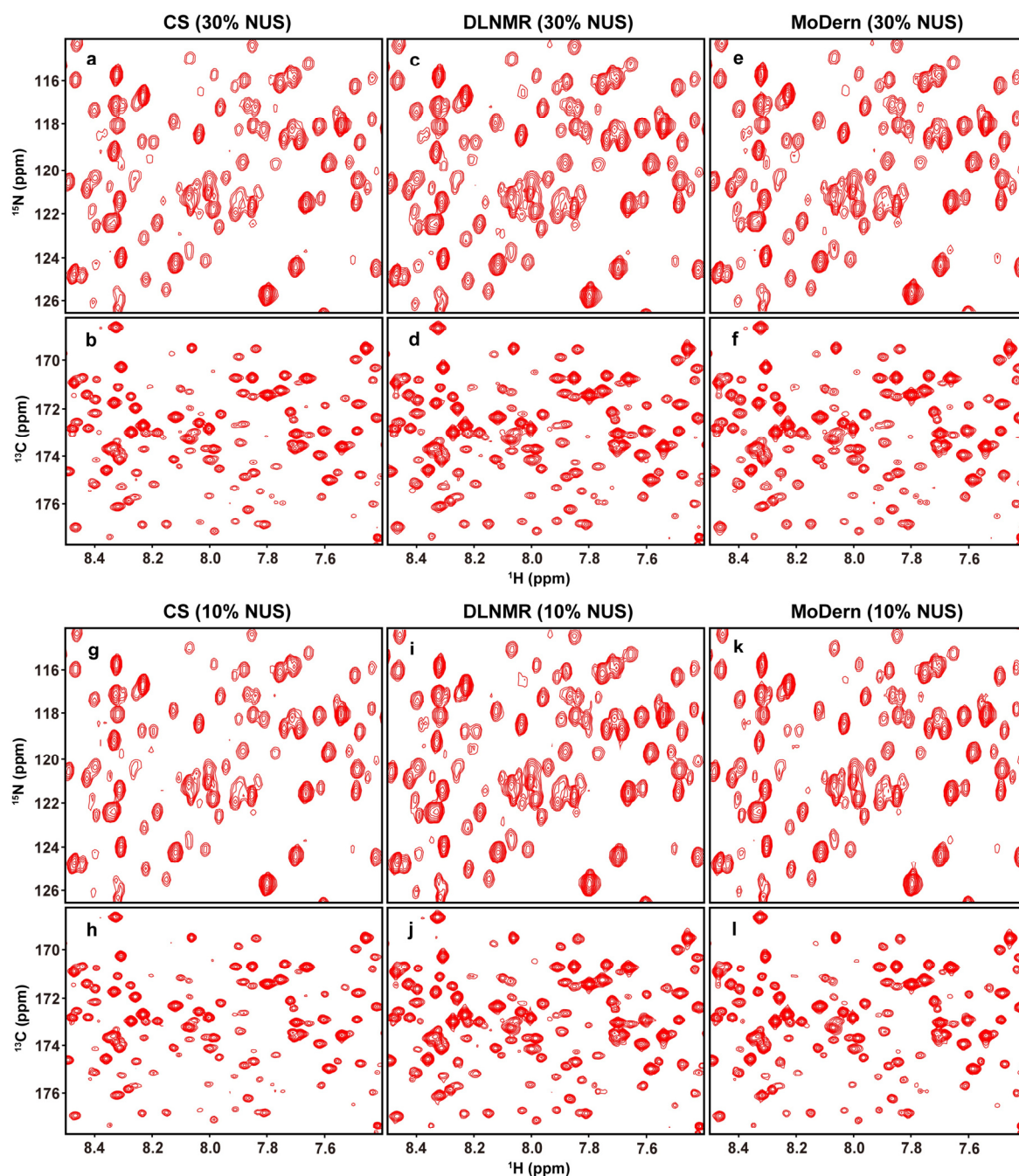


**Figure S3-6.** The sub-region of the projections on  $^1\text{H}$ - $^{15}\text{N}$  and  $^1\text{H}$ - $^{13}\text{C}$  planes of the 3D  $^1\text{H}$ - $^{15}\text{N}$  HNCOSY spectrum of MALT1 protein. (a-b), (c-d), and (e-f) are projections of the reconstructed spectrum using CS, DLNMR, and MoDern from 30% NUS data, respectively. (g-h), (i-j), and (k-l) are projections of the reconstructed spectrum using CS, DLNMR, and MoDern from 10% NUS data, respectively.



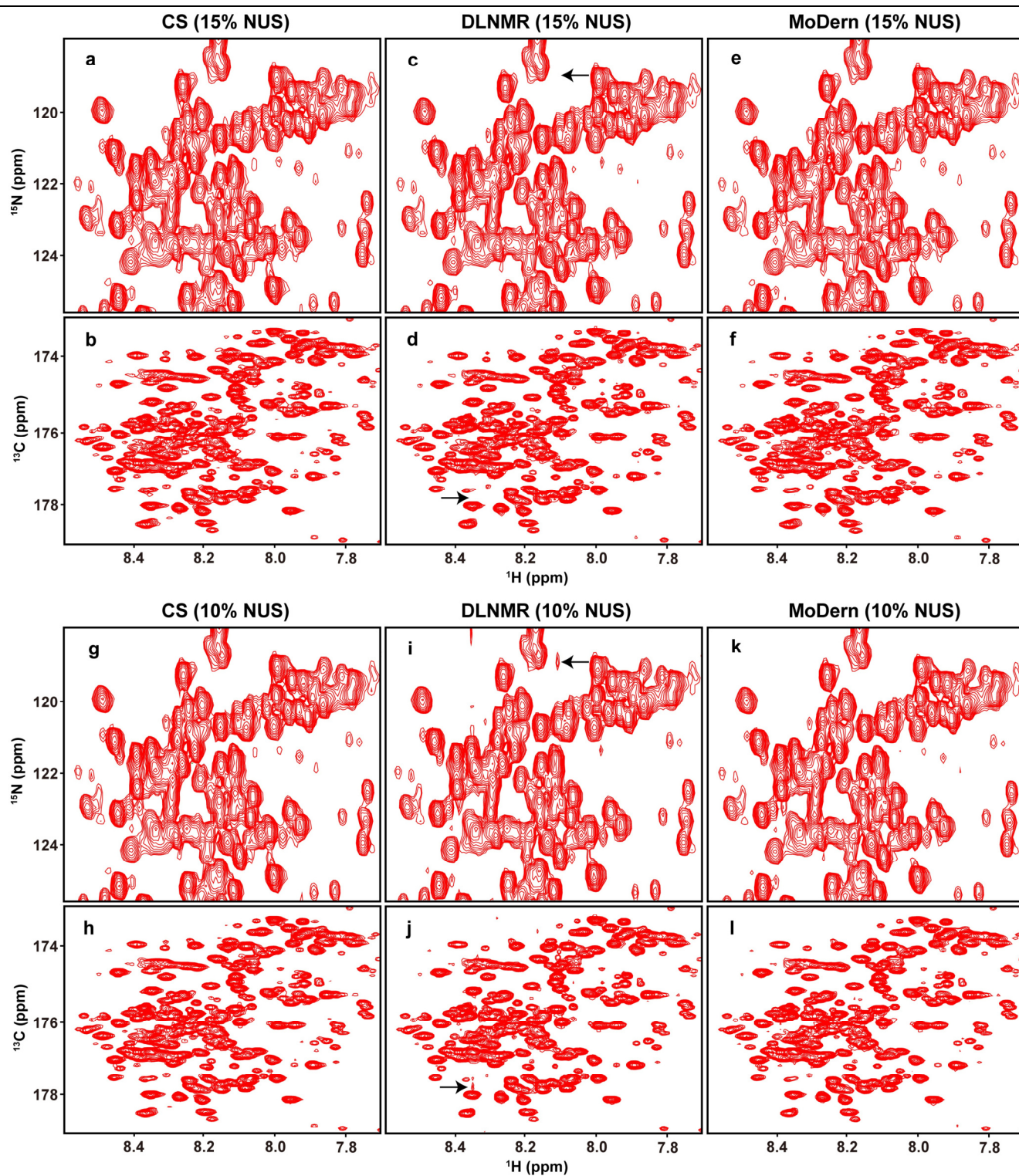


**Figure S3-7.** The sub-region of the projections on  $^1\text{H}$ - $^{15}\text{N}$  and  $^1\text{H}$ - $^{13}\text{C}$  planes of the 3D  $^1\text{H}$ - $^{15}\text{N}$  HNCO spectrum of Alpha-synuclein protein. (a-b), (c-d), and (e-f) are projections of the reconstructed spectrum using CS, DLNMR, and MoDern from 15% NUS data, respectively. (g-h), (i-j), and (k-l) are projections of the reconstructed spectrum using CS, DLNMR, and MoDern from 10% NUS data, respectively. Note: The artifacts in (i-j) are marked with the black arrow.

---

## Supporting Information S4. Comparison with CS on effective sensitivity

Effective sensitivity of reconstruction methods is defined as a possibility to detect weak peaks and discriminate them from eventual false signals<sup>[13]</sup>.

Figure S4-1(A) shows a comparison between a synthetic fully sampled reference spectrum and its NUS reconstructions obtained using CS<sup>[5a]</sup>, and MoDern. The spectrum contains five peaks with different line widths. It can be observed that while the narrow Peak 3-5 are successfully recovered, the other two peaks have visible distortions exacerbated as the peaks get broader and weaker, while MoDern reconstructs all five peaks faithfully. This conclusion is further verified by much higher peak intensity correlations obtained by MoDern on Peak 1 and 2, when the NUS density is in the range 10%~20%.

In Figure S4-1(B), the results on a 2D  $^1\text{H}$ - $^{15}\text{N}$  HSQC spectrum of the cytosolic domain of CD79b, are highly consistent with the synthetic data. We first observe qualitatively that the spectrum reconstructed by MoDern is more similar to fully sampled spectrum, which is corroborated by the higher peak intensity correlations than CS. Second, after zooming out 1D  $^{15}\text{N}$  traces to show the lineshapes, we find that several weak peaks are significantly distorted in the CS reconstruction, while it does not occur in the MoDern. And for the general peaks, both methods have good reconstruction.

Thus, we can conclude that, MoDern produces at least as good spectra reconstruction as CS and often outperforms it for broadest and weakest peaks, which indicate high effective sensitivity of MoDern.

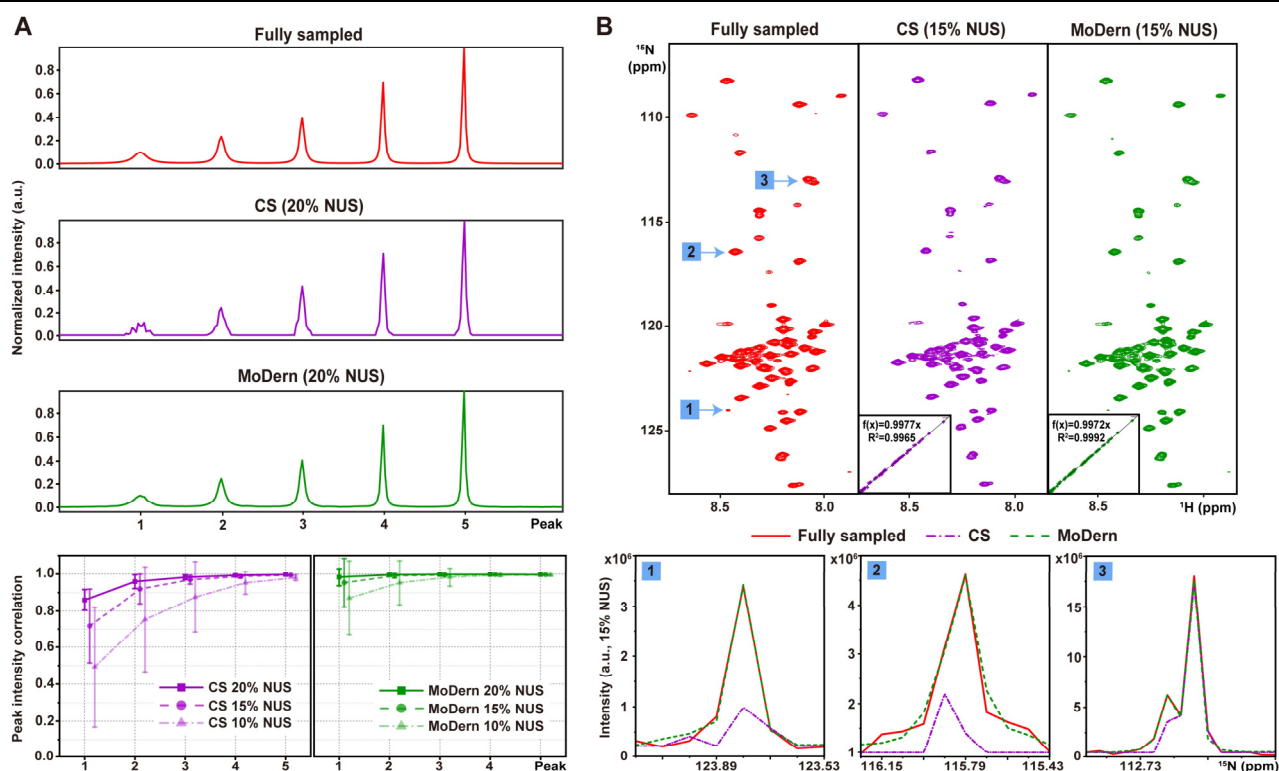


**Figure S4-1.** Evaluation on effective sensitivity of MoDern. (A) Reconstruction of the synthetic spectrum with five peaks. The top three are the fully sampled spectrum, reconstructed spectra using CS and MoDern from 20% data, respectively. The bottom are the peak intensity correlations between fully sampled spectrum and reconstructed spectrum using CS and MoDern under different NUS densities, respectively. The average and standard deviations of correlations are computed over 100 NUS trials. (B) Reconstruction of 2D  $^1\text{H}$ - $^{15}\text{N}$  HSQC spectrum of the cytosolic domain of CD79b. The top, from left to right are the fully sampled spectrum, reconstructed spectra using CS and MoDern from 15% data, respectively. The bottom, from left to right are zoomed out 1D  $^{15}\text{N}$  traces to show the lineshapes. The insets of reconstructed spectra show the peak intensity correlations between fully sampled spectrum and reconstructed spectrum. Note: The  $R^2$  denotes the square of Pearson correlation coefficient.

---

## Supporting Information S5. Further discussion on the robustness of MoDern

In accelerated NMR spectroscopy, the existing data-driven deep learning methods<sup>[1, 14]</sup> have strong dependence on training datasets, and have weak robustness and universality. Herein, we will focus on the applicability and compatibility of the proposed MoDern, to explore another important benefit of merging optimization and deep learning, in addition to the clarity of network structures and the greatly reduction of network parameters.

The strong applicability of MoDern to the spectra size and type has been demonstrated through multiple sets of reconstruction experiments in Supporting Information S3. In Supporting Information S3, for the same spectra dimensionality (2D or 3D) and NUS density, all reconstruction results are obtained by the same MoDern network, without re-training.

Next, we will discuss the compatibility of the proposed MoDern to different NUS densities. Among all reconstruction results in a 1D synthetic spectrum (Figure S5-1) and realistic 2D/3D NMR spectra (Figure S5-2, S5-3, S5-4, S5-5, S5-6), it can be seen that the state-of-the-art data-driven deep learning method, DLNMR<sup>[1]</sup>, shows a significant performance decline if the NUS density of the spectrum is far from trained one. However, MoDern can maintain the stable and reliable performance, due to the introduction of reasonable sparse prior relaxing its dependence on the training dataset.

In summary, MoDern can overcome the mismatch between training datasets and targets, leading to work effectively in a wide range of scenarios without re-training.

### 1D synthetic spectrum

For 1D synthetic spectrum, MoDern is compared with a representative NUS NMR reconstruction methods, the data-driven deep learning method (DLNMR<sup>[1]</sup>). To demonstrate the applicability and compatibility of the trained MoDern, we reconstruct a synthetic spectrum with five peaks, which is introduced in Figure S4-1(A).

In Figure S5-1, MoDern can maintain the high-quality reconstruction performance even the NUS density of the spectrum is far from trained one, and lineshapes of the spectra closing to the fully sampled spectra can demonstrate this. However, DLNMR shows the significant performance decline, e.g., peak intensity distortions and artifacts, which can be seen reflected in intensity correlations of Peak 1 and reconstructed spectra.



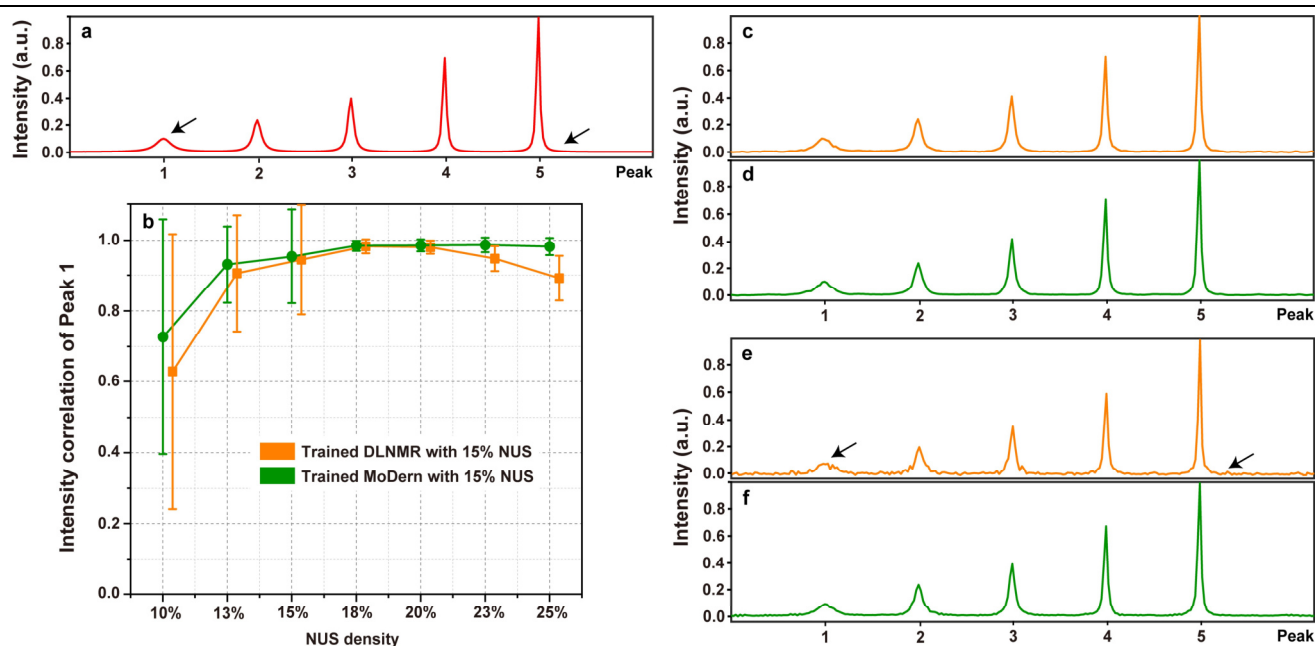


**Figure S5-1.** The reconstruction results of the trained MoDern, and the trained DLNMR from varied NUS density for 1D synthetic spectrum with five peaks. (a) The fully sampled spectrum. (b) The correlations of DLNMR and MoDern trained using 15% NUS density dataset respectively, to reconstruct the broadest Peak 1 of spectra sampled under a series of NUS densities ranging from 10% to 25%. (c) and (e) are the typical of reconstructed results of DLNMR trained using 25% and 15% NUS density datasets, respectively, to reconstruct spectra from 25% data. (d) and (f) are the typical of reconstructed results of MoDern trained using 25% and 15% NUS density datasets, respectively, to reconstruct spectra from 25% data. Note: The average and standard deviations of correlations in (b) are computed over 100 NUS trials. The peak intensity correlations of DLNMR (orange line) are shifted horizontally for clear display but the values unchanged. The intensity distortions and artifacts in (e) are marked with the black arrow.

## 2D NMR spectra

For 2D NMR spectra, MoDern is compared with a representative NUS NMR reconstruction methods, the data-driven deep learning method (DLNMR<sup>[1]</sup>). To demonstrate the applicability and compatibility of the trained MoDern, we reconstruct three spectra, which are introduced in Supporting Information S2.

For the reconstruction of two spectra with moderate dynamic range (Figure S5-2 and S5-3), MoDern can maintain the high-quality reconstruction performance even the NUS density of the spectrum is far from trained one, and very high peak intensity correlations ( $>0.999$ ) can demonstrate this. However, DLNMR shows the significant performance decline, e.g., peak intensity distortions and artifacts, which can be seen reflected in peak intensity correlations and reconstructed spectra.

For the reconstruction of a high dynamic range NOESY spectrum with many weak peaks (Figure S5-4), MoDern also have the stable and reliable performance, and can maintain the high peak intensity correlation ( $>0.99$ ) even on low-intensity peaks, while as we mentioned before, DLNMR fails to handle this scenario.

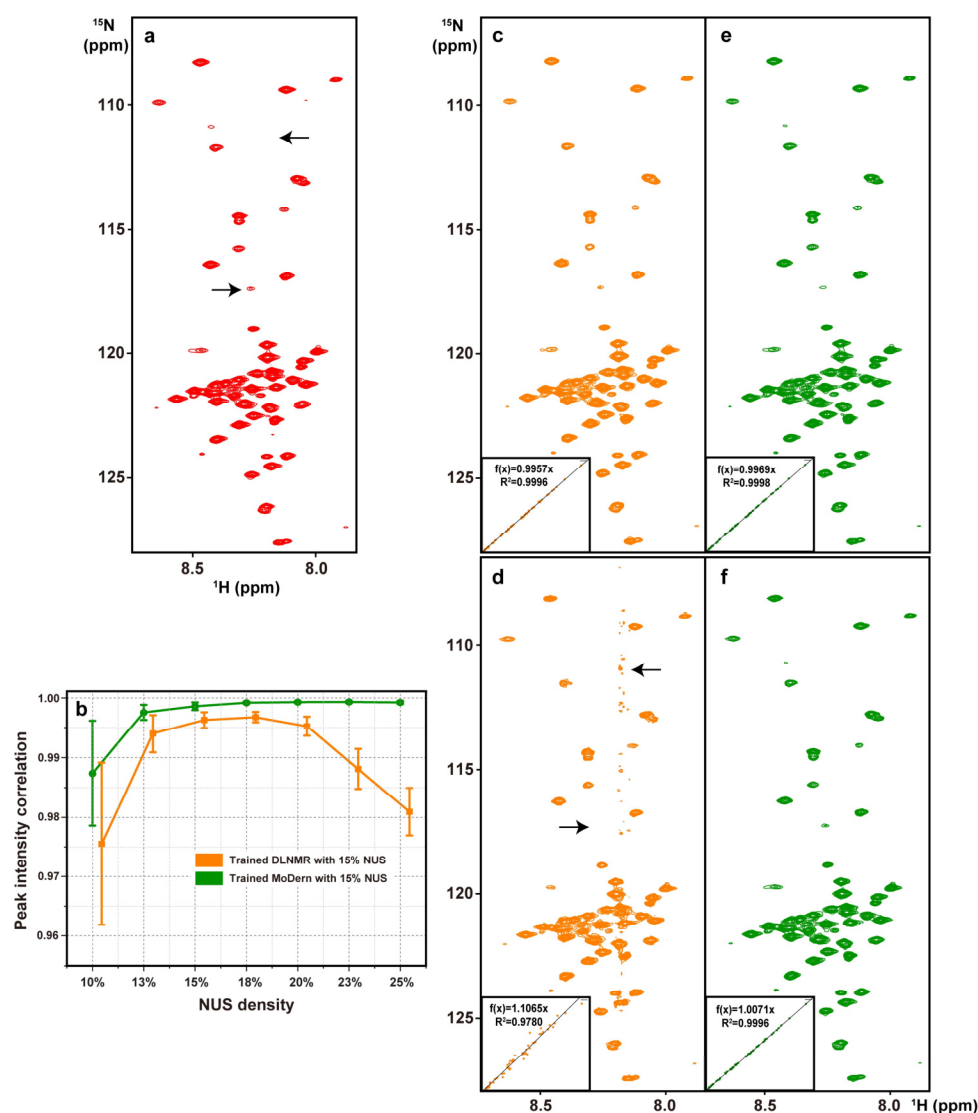


**Figure S5-2.** The reconstruction results of the trained MoDern, and the trained DLNMR from varied NUS density for 2D  $^1\text{H}$ - $^{15}\text{N}$  HSQC spectrum of CD79b. (a) The fully sampled spectrum. (b) The correlations of DLNMR and MoDern trained using 15% NUS density dataset respectively, to reconstruct spectra sampled under a series of NUS densities ranging from 10% to 25%. (c) and (d) are the typical of reconstructed results of DLNMR trained using 25% and 15% NUS density datasets, respectively, to reconstruct spectra from 25% data. (e) and (f) are the typical of reconstructed results of MoDern trained using 25% and 15% NUS density datasets, respectively, to reconstruct spectra from 25% data. The insets of (c-f) show the peak intensity correlation between fully sampled spectrum and reconstructed spectrum. Note: The  $R^2$  denotes the square of Pearson correlation coefficient. The average and standard deviations of correlations in (b) are computed over 100 NUS trials. The peak intensity correlations of DLNMR (orange line) are shifted horizontally for clear display but the values unchanged. The intensity distortions and artifacts in (d) are marked with the black arrow.

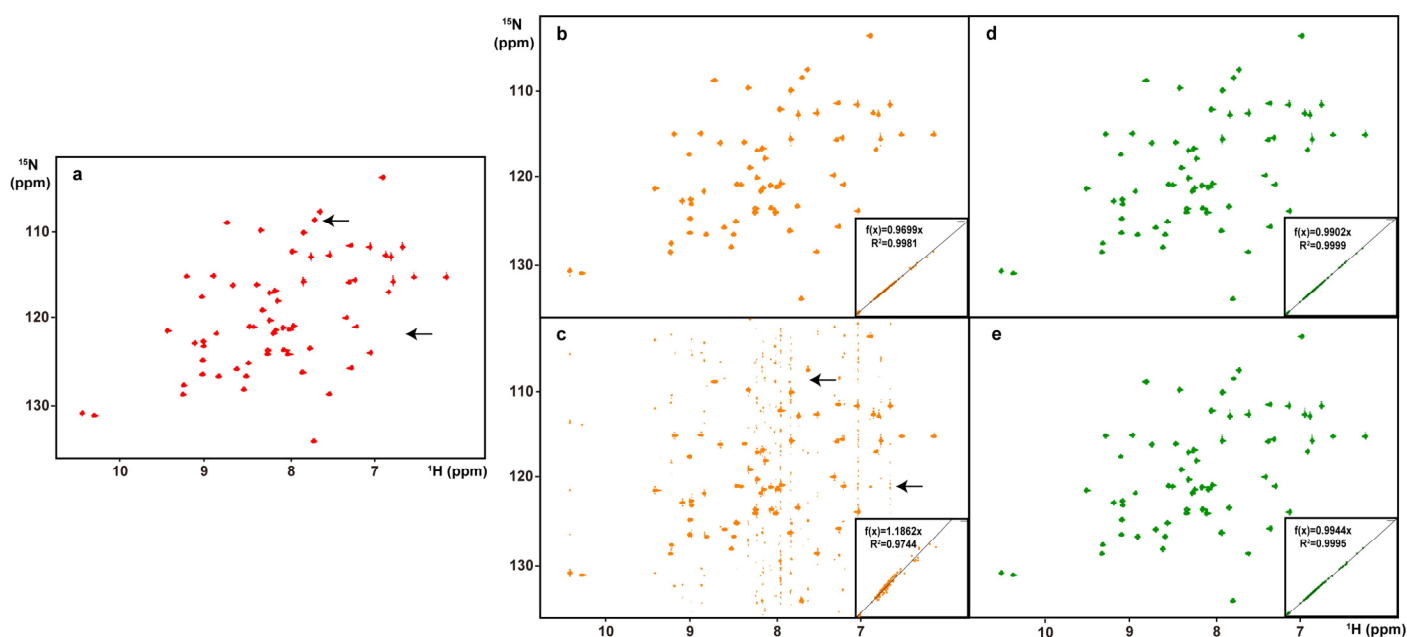


**Figure S5-3.** The reconstruction results of the trained MoDern, and the trained DLNMR from varied NUS density for 2D  $^1\text{H}$ - $^{15}\text{N}$  HSQC spectrum of Gb1. (a) The fully sampled spectrum. (b) and (c) are the typical of reconstructed results of DLNMR trained using 25% and 15% NUS density datasets, respectively, to reconstruct spectra from 25% data. (d) and (e) are the typical of reconstructed results of MoDern trained using 25% and 15% NUS density datasets, respectively, to reconstruct spectra from 25% data. The insets of (b-e) show the peak intensity correlation between fully sampled spectrum and reconstructed spectrum. Note: The intensity distortions and artifacts in (c) are marked with the black arrow.

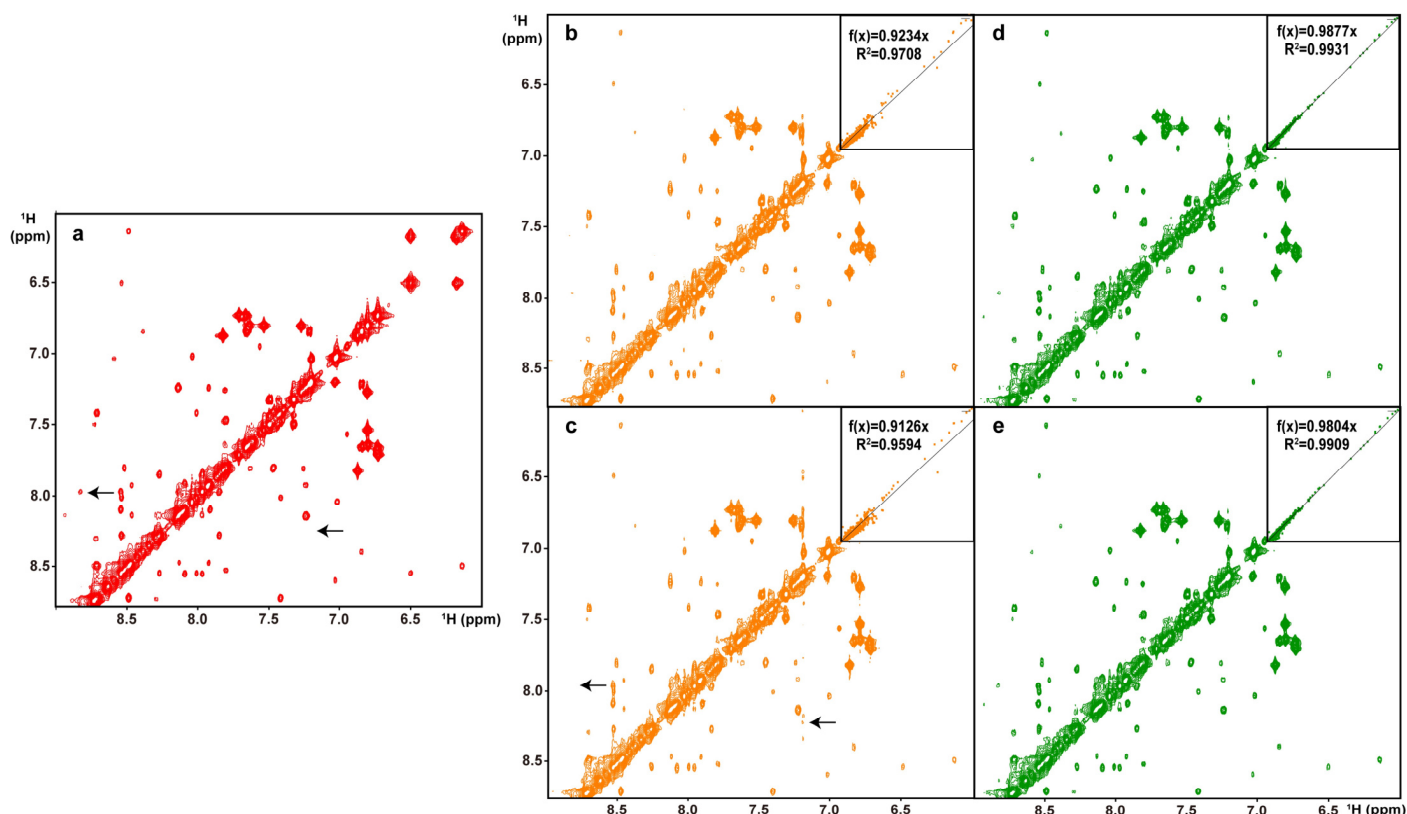


**Figure S5-4.** The reconstruction results of the trained MoDern, and the trained DLNMR from varied NUS density for 2D  $^1\text{H}$ - $^1\text{H}$  NOESY spectrum of human ubiquitin. (a) The fully sampled spectrum. (b) and (c) are the typical of reconstructed results of DLNMR trained using 40% and 30% NUS density datasets, respectively, to reconstruct spectra from 40% data. (d) and (e) are the typical of reconstructed results of MoDern trained using 40% and 30% NUS density datasets, respectively, to reconstruct spectra from 40% data. The insets of (b-e) show the peak intensity correlation between fully sampled spectrum and reconstructed spectrum. Note: The intensity distortions and artifacts in (c) are marked with the black arrow.

### 3D NMR spectra

For 3D NMR spectra, MoDern is also compared with a representative NUS NMR reconstruction methods, the data-driven deep learning method (DLNMR<sup>[1]</sup>). To demonstrate the applicability and compatibility of the trained MoDern, we reconstruct two spectra, which are introduced in Supporting Information S2.

In Figure S5-5 and S5-6, MoDern can maintain the high-quality reconstruction performance even the NUS density of the spectrum is far from trained one, and very high peak intensity correlations ( $>0.996$ ) can demonstrate this. However, DLNMR shows the performance decline, e.g., peak intensity distortions and artifacts, which can be seen reflected in reconstructed spectra.

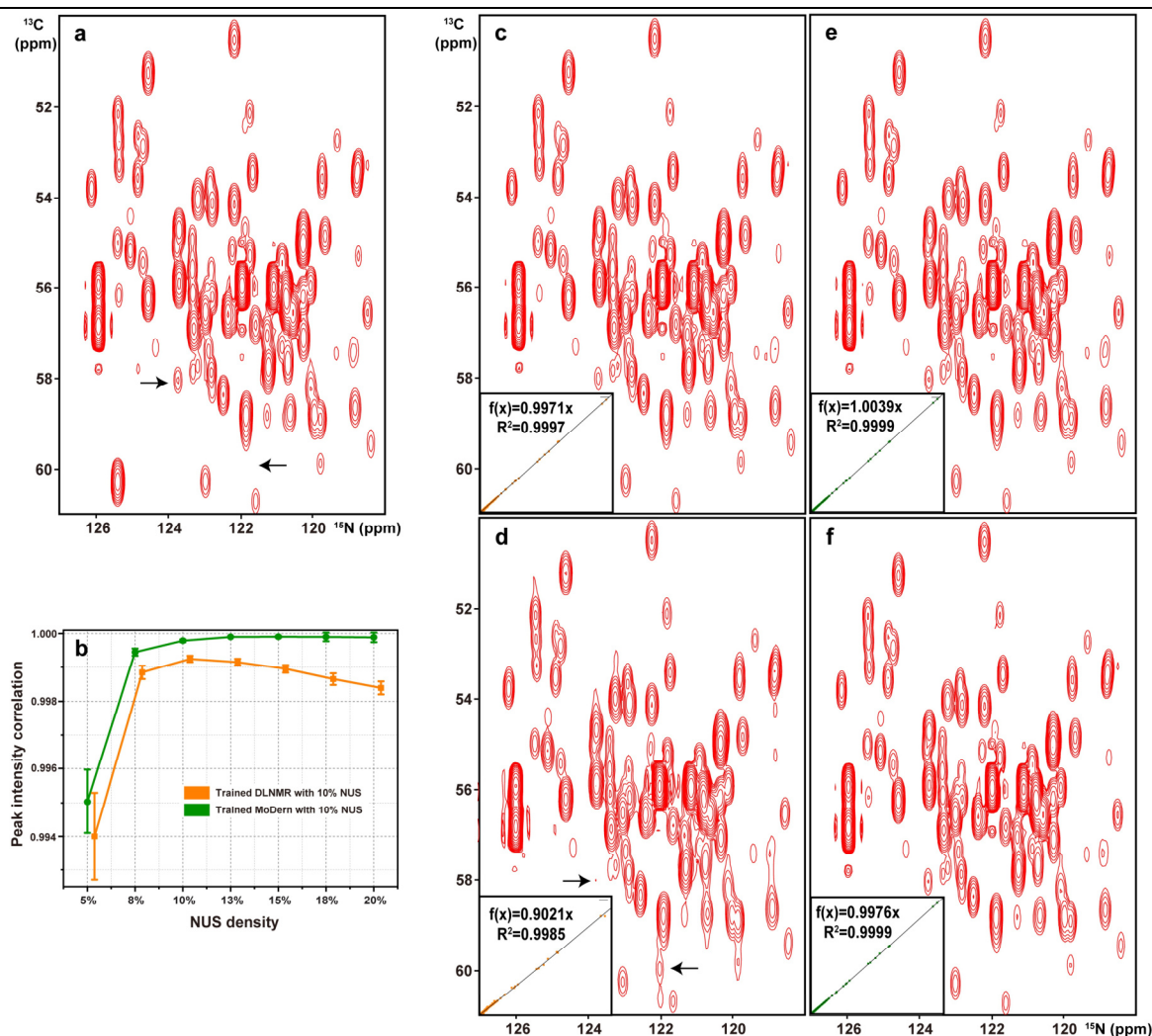


**Figure S5-5.** The reconstructed sub-region of the projections on  $^{13}\text{C}$ - $^{15}\text{N}$  planes of the trained MoDern, and the trained DLNMR from varied NUS density for 3D HNCACB spectrum of GB1-HttNTQ7. (a) The fully sampled spectrum. (b) The correlations of DLNMR and MoDern trained using 10% NUS density dataset respectively, to reconstruct spectra sampled under a series of NUS densities ranging from 5% to 20%. (c) and (d) are the typical of reconstructed results of DLNMR trained using 20% and 10% NUS density datasets, respectively, to reconstruct spectra from 20% data. (e) and (f) are the typical of reconstructed results of MoDern trained using 20% and 10% NUS density datasets, respectively, to reconstruct spectra from 20% data. The insets of (c-f) show the peak intensity correlation between fully sampled spectrum and reconstructed spectrum. Note: The average and standard deviations of correlations in (b) are computed over 50 NUS trials. The peak intensity correlations of DLNMR (orange line) are shifted horizontally for clear display but the values unchanged. The intensity distortions and artifacts in (d) are marked with the black arrow.

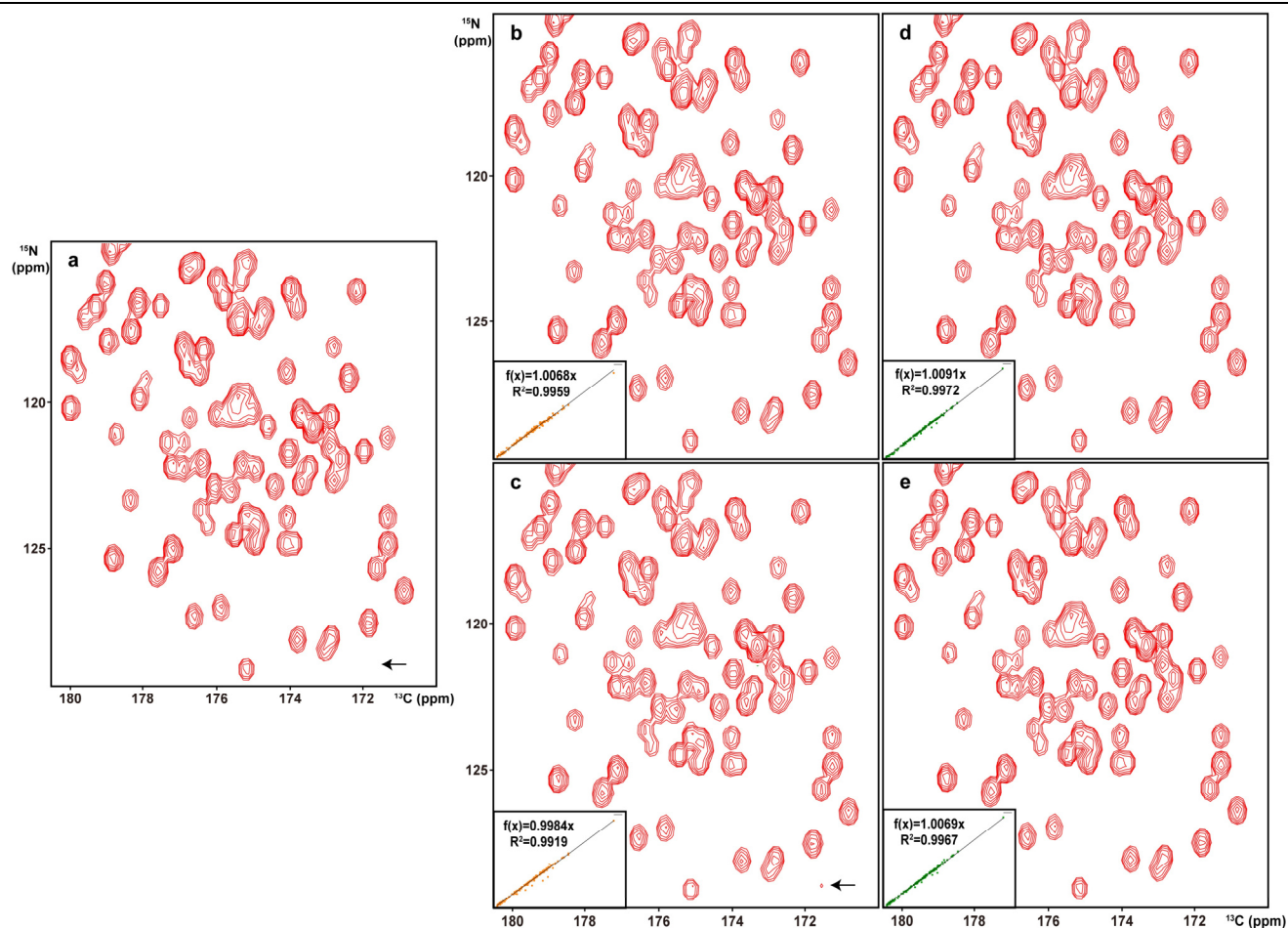


**Figure S5-6.** The reconstructed sub-region of the projections on  $^{15}\text{N}$ - $^{13}\text{C}$  planes of the trained MoDern, and the trained DLNMR from varied NUS density for 3D HNCOSY spectrum of Azurin. (a) The fully sampled spectrum. (b) and (c) are the typical of reconstructed results of DLNMR trained using 20% and 10% NUS density datasets, respectively, to reconstruct spectra from 20% data. (d) and (e) are the typical of reconstructed results of MoDern trained using 20% and 10% NUS density datasets, respectively, to reconstruct spectra from 20% data. The insets of (b-e) show the peak intensity correlation between fully sampled spectrum and reconstructed spectrum. The intensity distortion in (c) is marked with the black arrow.



## Supporting Information S6. Quantitative measurement on concentration of a mixture

The quantitative measurement on the relative concentration is analyzed on the 2D  $^1\text{H}$ - $^{13}\text{C}$  HSQC spectra of a mixture of three metabolites, including D-Glucose,  $\beta$ -Alanine and Valine. The HSQC spectra are obtained through a linear regression extrapolation<sup>[15]</sup>:

$$\ln(A_{i,n}) = \ln(A_{0,n}) + i \times \ln(f_{A,n}), \quad i = 1, 2, 3, \quad (\text{S6-1})$$

where  $A_{i,n}$  is the peak volume (the integrated signal intensity) of the  $n^{\text{th}}$  peak in HSQC <sub>$i$</sub> , and  $A_{0,n}$  is the peak volume of the  $n^{\text{th}}$  peak in time-zero HSQC<sub>0</sub>. Notably, the  $A_{0,n}$  is free of attenuation during the coherence transfer period, and  $f_{A,n}$  is the amplitude attenuation factor for the  $n^{\text{th}}$  peak<sup>[15]</sup>. Therefore, the  $A_{0,n}$  is chosen as the criteria to measure the relative concentration of metabolites.

Twelve cross peaks are chosen to measure the relative concentration, which is calculated as the ratio of the volume of a metabolite over the volume of the Valine (Figure S6-1). Furthermore, to improve the relative concentration of the mixture, we average the peak intensity of individual metabolites.

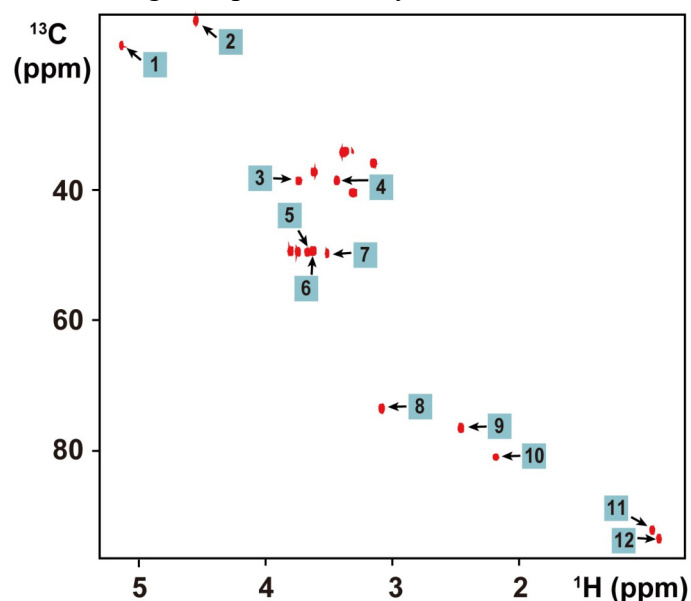


**Figure S6-1.** Spectral peak attribution for a mixture of three metabolites. Here, twelve cross-peaks are labelled. Among them, Peaks 1-6 are assigned to D-Glucose, Peaks 8-9 are assigned to  $\beta$ -Alanine, and Peaks 7, and 10-12 are assigned to Valine.

Relative concentrations of a mixture (three metabolites, including D-Glucose,  $\beta$ -Alanine and Valine), estimated from fully sampled spectra, and reconstructed spectra using CS, DLNMR, and MoDern from 20% NUS data, respectively, are reported below in Table S6-1, S6-2, S6-3, S6-4.



**Table S6-1.** Extrapolated peak volumes ( $A_0$ ) and measured peak volumes ( $A_1, A_2, A_3$ ) from fully sampled 2D HSQC<sub>*i*</sub> (*i* = 1, 2, 3) spectra. The peak volume  $A_{0,n}$  of the  $n^{th}$  peak in HSQC<sub>0</sub> is extrapolated from those volumes of the corresponding peak in HSQC<sub>1</sub>, HSQC<sub>2</sub>, and HSQC<sub>3</sub> following Eq. (S6-1). Peaks 1, 3, 4, 5 are assigned to D-Glucose ( $\alpha$ ) while peaks 2 and 6 are assigned to D-Glucose ( $\beta$ ). The volume of D-Glucose is the sum of those of D-Glucose ( $\alpha$ ) and D-Glucose ( $\beta$ ). The ratio D-Glucose:  $\beta$ -Alanine: Valine = 6.87: 3.62: 1.51  $\approx$  4.55:2.40:1.00.

Metabolites		Peak ID	Peak volumes					
			Measured on spectra			Extrapolated from HSQC <sub><i>i</i></sub> ( <i>i</i> =1,2,3)		
			HSQC <sub>1</sub>	HSQC <sub>2</sub>	HSQC <sub>3</sub>	HSQC <sub>0</sub>	Average	Standard deviation
D-Glucose	α	1	2.05×10 <sup>9</sup>	9.08×10 <sup>8</sup>	3.60×10 <sup>8</sup>	2.80×10 <sup>9</sup>	2.65×10 <sup>9</sup>	1.34×10 <sup>8</sup>
		3	1.90×10 <sup>9</sup>	9.33×10 <sup>8</sup>	3.76×10 <sup>8</sup>	2.59×10 <sup>9</sup>		
		4	1.86×10 <sup>9</sup>	9.04×10 <sup>8</sup>	4.21×10 <sup>8</sup>	2.50×10 <sup>9</sup>		
		5	2.02×10 <sup>9</sup>	9.92×10 <sup>8</sup>	4.35×10 <sup>8</sup>	2.73×10 <sup>9</sup>		
	β	2	3.13×10 <sup>9</sup>	1.39×10 <sup>9</sup>	4.74×10 <sup>8</sup>	4.32×10 <sup>9</sup>	4.22×10 <sup>9</sup>	1.48×10 <sup>8</sup>
		6	3.14×10 <sup>9</sup>	1.55×10 <sup>9</sup>	8.89×10 <sup>8</sup>	4.11×10 <sup>9</sup>		
β-Alanine		8	5.20×10 <sup>9</sup>	2.69×10 <sup>9</sup>	1.27×10 <sup>9</sup>	3.49×10 <sup>9</sup>	3.62×10 <sup>9</sup>	1.79×10 <sup>8</sup>
		9	5.53×10 <sup>9</sup>	2.71×10 <sup>9</sup>	1.18×10 <sup>9</sup>	3.75×10 <sup>9</sup>		
Valine		7	1.37×10 <sup>9</sup>	6.94×10 <sup>8</sup>	3.70×10 <sup>8</sup>	1.81×10 <sup>9</sup>	1.51×10 <sup>9</sup>	2.03×10 <sup>8</sup>
		10	1.05×10 <sup>9</sup>	4.97×10 <sup>8</sup>	1.93×10 <sup>8</sup>	1.44×10 <sup>9</sup>		
		11	3.06×10 <sup>9</sup>	1.25×10 <sup>9</sup>	4.63×10 <sup>8</sup>	1.40×10 <sup>9</sup>		
		12	3.05×10 <sup>9</sup>	1.22×10 <sup>9</sup>	4.52×10 <sup>8</sup>	1.39×10 <sup>9</sup>		

**Table S6-2.** Extrapolated peak volumes ( $A_0$ ) and measured peak volumes ( $A_1, A_2, A_3$ ) from reconstructed 2D HSQC $_i$  ( $i = 1, 2, 3$ ) spectra using CS from 20% NUS data. The ratio D-Glucose:  $\beta$ -Alanine: Valine = 6.67: 3.51: 1.43  $\approx$  4.66:2.45:1.00.

Metabolites		Peak ID	Peak volumes					
			Measured on spectra			Extrapolated from HSQC <sub><i>i</i></sub> ( <i>i</i> =1,2,3)		
			HSQC <sub>1</sub>	HSQC <sub>2</sub>	HSQC <sub>3</sub>	HSQC <sub>0</sub>	Average	Standard deviation
D-Glucose	α	1	1.95×10 <sup>9</sup>	8.57×10 <sup>8</sup>	3.16×10 <sup>8</sup>	2.68×10 <sup>9</sup>	2.61×10 <sup>9</sup>	1.14×10 <sup>8</sup>
		3	1.95×10 <sup>9</sup>	8.76×10 <sup>8</sup>	3.43×10 <sup>8</sup>	2.66×10 <sup>9</sup>		
		4	1.81×10 <sup>9</sup>	8.60×10 <sup>8</sup>	3.93×10 <sup>8</sup>	2.44×10 <sup>9</sup>		
		5	1.94×10 <sup>9</sup>	9.99×10 <sup>8</sup>	3.96×10 <sup>8</sup>	2.66×10 <sup>9</sup>		
	β	2	2.97×10 <sup>9</sup>	1.35×10 <sup>9</sup>	4.40×10 <sup>8</sup>	4.12×10 <sup>9</sup>	4.06×10 <sup>9</sup>	8.34×10 <sup>7</sup>
		6	2.99×10 <sup>9</sup>	1.75×10 <sup>9</sup>	8.57×10 <sup>8</sup>	4.00×10 <sup>9</sup>		
β-Alanine		8	5.02×10 <sup>9</sup>	2.63×10 <sup>9</sup>	1.24×10 <sup>9</sup>	3.37×10 <sup>9</sup>	3.51×10 <sup>9</sup>	1.92×10 <sup>8</sup>
		9	5.38×10 <sup>9</sup>	2.64×10 <sup>9</sup>	1.15×10 <sup>9</sup>	3.64×10 <sup>9</sup>		
Valine		7	1.33×10 <sup>9</sup>	6.30×10 <sup>8</sup>	3.37×10 <sup>8</sup>	1.76×10 <sup>9</sup>	1.43×10 <sup>9</sup>	2.25×10 <sup>8</sup>
		10	9.18×10 <sup>8</sup>	4.19×10 <sup>8</sup>	1.69×10 <sup>8</sup>	1.25×10 <sup>9</sup>		
		11	2.95×10 <sup>9</sup>	1.20×10 <sup>9</sup>	4.26×10 <sup>8</sup>	1.35×10 <sup>9</sup>		
		12	2.98×10 <sup>9</sup>	1.15×10 <sup>9</sup>	4.17×10 <sup>8</sup>	1.36×10 <sup>9</sup>		

**Table S6-3.** Extrapolated peak volumes ( $A_0$ ) and measured peak volumes ( $A_1, A_2, A_3$ ) from reconstructed 2D HSQC $_i$  ( $i = 1, 2, 3$ ) spectra using DLNMR from 20% NUS data. The ratio D-Glucose:  $\beta$ -Alanine: Valine = 6.94: 3.56: 1.47  $\approx$  4.56:2.42:1.00.

Metabolites		Peak ID	Peak volumes					
			Measured on spectra			Extrapolated from HSQC <sub>i</sub> (i=1,2,3)		
			HSQC <sub>1</sub>	HSQC <sub>2</sub>	HSQC <sub>3</sub>	HSQC <sub>0</sub>	Average	Standard deviation
D-Glucose	α	1	1.97×10 <sup>9</sup>	8.74×10 <sup>8</sup>	3.28×10 <sup>8</sup>	2.70×10 <sup>9</sup>	2.56×10 <sup>9</sup>	1.17×10 <sup>8</sup>
		3	1.90×10 <sup>9</sup>	9.31×10 <sup>8</sup>	3.57×10 <sup>8</sup>	2.61×10 <sup>9</sup>		
		4	1.79×10 <sup>9</sup>	9.19×10 <sup>8</sup>	4.03×10 <sup>8</sup>	2.42×10 <sup>9</sup>		
		5	1.86×10 <sup>9</sup>	1.02×10 <sup>9</sup>	4.36×10 <sup>8</sup>	2.53×10 <sup>9</sup>		
	β	2	3.01×10 <sup>9</sup>	1.39×10 <sup>9</sup>	5.06×10 <sup>8</sup>	4.14×10 <sup>9</sup>	4.38×10 <sup>9</sup>	3.44×10 <sup>8</sup>
		6	3.46×10 <sup>9</sup>	1.75×10 <sup>9</sup>	8.57×10 <sup>8</sup>	4.63×10 <sup>9</sup>		
β-Alanine		8	5.06×10 <sup>9</sup>	2.64×10 <sup>9</sup>	1.24×10 <sup>9</sup>	3.40×10 <sup>9</sup>	3.56×10 <sup>9</sup>	2.32×10 <sup>8</sup>
		9	5.51×10 <sup>9</sup>	2.65×10 <sup>9</sup>	1.16×10 <sup>9</sup>	3.73×10 <sup>9</sup>		
Valine		7	1.35×10 <sup>9</sup>	6.49×10 <sup>8</sup>	3.46×10 <sup>8</sup>	1.79×10 <sup>9</sup>	1.47×10 <sup>9</sup>	2.10×10 <sup>8</sup>
		10	1.01×10 <sup>9</sup>	4.79×10 <sup>8</sup>	1.88×10 <sup>8</sup>	1.38×10 <sup>9</sup>		
		11	2.97×10 <sup>9</sup>	1.21×10 <sup>9</sup>	4.48×10 <sup>8</sup>	1.35×10 <sup>9</sup>		
		12	2.99×10 <sup>9</sup>	1.17×10 <sup>9</sup>	4.29×10 <sup>8</sup>	1.36×10 <sup>9</sup>		

**Table S6-4.** Extrapolated peak volumes ( $A_0$ ) and measured peak volumes ( $A_1, A_2, A_3$ ) from reconstructed 2D HSQC $_i$  ( $i = 1, 2, 3$ ) spectra using MoDern from 20% NUS data. The ratio D-Glucose:  $\beta$ -Alanine: Valine = 6.73: 3.55: 1.48  $\approx$  4.55:2.40:1.00.

Metabolites		Peak ID	Peak volumes					
			Measured on spectra			Extrapolated from HSQC <sub>i</sub> (i=1,2,3)		
			HSQC <sub>1</sub>	HSQC <sub>2</sub>	HSQC <sub>3</sub>	HSQC <sub>0</sub>	Average	Standard deviation
D-Glucose	α	1	2.02×10 <sup>9</sup>	8.78×10 <sup>8</sup>	3.49×10 <sup>8</sup>	2.75×10 <sup>9</sup>	2.59×10 <sup>9</sup>	1.74×10 <sup>8</sup>
		3	1.83×10 <sup>9</sup>	8.88×10 <sup>8</sup>	3.56×10 <sup>8</sup>	2.50×10 <sup>9</sup>		
		4	1.77×10 <sup>9</sup>	8.75×10 <sup>8</sup>	3.94×10 <sup>8</sup>	2.39×10 <sup>9</sup>		
		5	2.00×10 <sup>9</sup>	9.77×10 <sup>8</sup>	4.16×10 <sup>8</sup>	2.72×10 <sup>9</sup>		
	β	2	3.05×10 <sup>9</sup>	1.19×10 <sup>9</sup>	3.35×10 <sup>8</sup>	4.24×10 <sup>9</sup>	4.14×10 <sup>9</sup>	1.45×10 <sup>8</sup>
		6	3.07×10 <sup>9</sup>	1.53×10 <sup>9</sup>	8.52×10 <sup>8</sup>	4.04×10 <sup>9</sup>		
β-Alanine		8	5.10×10 <sup>9</sup>	2.67×10 <sup>9</sup>	1.26×10 <sup>9</sup>	3.43×10 <sup>9</sup>	3.55×10 <sup>9</sup>	1.72×10 <sup>8</sup>
		9	5.42×10 <sup>9</sup>	2.65×10 <sup>9</sup>	1.16×10 <sup>9</sup>	3.67×10 <sup>9</sup>		
Valine		7	1.35×10 <sup>9</sup>	6.87×10 <sup>8</sup>	3.58×10 <sup>8</sup>	1.79×10 <sup>9</sup>	1.48×10 <sup>9</sup>	2.05×10 <sup>8</sup>
		10	1.00×10 <sup>9</sup>	4.70×10 <sup>8</sup>	1.41×10 <sup>8</sup>	1.40×10 <sup>9</sup>		
		11	3.02×10 <sup>9</sup>	1.21×10 <sup>9</sup>	4.27×10 <sup>8</sup>	1.38×10 <sup>9</sup>		
		12	2.99×10 <sup>9</sup>	1.17×10 <sup>9</sup>	4.15×10 <sup>8</sup>	1.37×10 <sup>9</sup>		

---

## Supporting Information S7. Setups of all methods and reconstruction time on local

In this section, we describe the setups and parameters of all methods shown in the paper. Herein, the reconstruction time of all methods on local is reported in Table S7-1.

All local experiments implemented on a server equipped with dual Intel Xeon CPUs (2.2 GHz, 24 cores in total), 128 GB RAM, and one Nvidia Tesla K40M GPU. The proposed MoDern is performed on Python 3.6 and Tensorflow 1.14.0<sup>[16]</sup> as backend, as well as DLNMR<sup>[1]</sup>. CS<sup>[5a]</sup> was implemented by using MATLAB 2018b with 24 threads for synthetic data and using MddNMR toolbox<sup>[5a]</sup> with 24 threads for realistic NMR data. The CS was parallelized with aspects to the direct dimensions to maximally reduce the computation time under multiple CPU cores, and the deep learning methods were trained under one GPU. The direct dimensions of all spectra were processed using NMRPipe<sup>[9]</sup>. After reconstruction, the indirection dimensions of reconstructed data were also processed in NMRPipe. Finally, the shown spectra were analyzed using SPARKY<sup>[17]</sup>.

CS does not require pre-training, and uses the IST algorithm with virtual echo (VE)<sup>[4]</sup> for optimal performance. For reconstructing synthetic data in MATLAB, its key parameters are as follows: lambda is  $2.2e5$ , maximum iteration is 300, and tolerance is  $1e-6$ . For reconstructing realistic NMR data in MddNMR, its key parameters are as follows: maximum iteration is 300.

DLNMR needs training before reconstruction. The network hyper-parameters are exactly the same as the original paper<sup>[1]</sup>. It is trained once under a given NUS density and spectra dimensionality, and then exploits for different spectra on different samples. The total training time are 10.4 hours and 43.7 hours for 2D and 3D NMR within 80 epochs, respectively.

MoDern reduces the network trainable parameters dramatically and reduces the computational complexity. It is also trained once under a given NUS density and spectra dimensionality, and then exploits for different spectra on different samples. The total training time are 3.9 hours and 15.1 hours for 2D and 3D NMR within 80 epochs, respectively, which is ca. 35% of that needed for DLNMR.

**Table S7-1.** Reconstruction time of CS, DLNMR, and MoDern (Unit: seconds). For 2D (3D) spectra, the size of the directly detected dimension is followed by the size(s) of the indirect dimension(s).

Spectra Type		Samples	Molecular weight	Spectra size	Reconstruction time on local		
					CS	DLNMR	MoDern
<b>2D</b>	HSQC	CD79b	5.7 kDa	116 × 256	0.29	0.08	<b>0.04</b>
	HSQC	Gbl	8.0 kDa	1146 × 170	3.32	0.62	<b>0.13</b>
	TROSY	Ubiquitin	8.6 kDa	512 × 128	1.22	0.17	<b>0.05</b>
	NOESY	Ubiquitin	7 kDa	928 × 512	1.39	0.85	<b>0.17</b>
<b>3D</b>	HNCACB	GB1-HttNTQ7	10 kDa	879 × 90 × 44	225.12	13.08	<b>3.18</b>
	HNCO	Azurin	14 kDa	732 × 60 × 60	44.84	9.44	<b>2.38</b>
	HNCO	MALT1	44 kDa	735 × 57 × 70	135.19	11.88	<b>2.75</b>
	HNCO	Alpha-synuclein	14.5 kDa	221 × 64 × 64	16.53	3.68	<b>0.78</b>

## Supporting Information S8. More Information about XCloud-MoDern

Cloud computing platform is generally web-based and easily accessible through a variety of internet-connected devices without installation. Through an easy-to-use interface, users can enjoy reliable, efficient, and high-performance experience.

Our XCloud-MoDern is for easily and fastly processing multi-dimensional NMR spectra. In the NUS acquisition, only a fraction of full data is recorded. Potentially, any pulse sequence can be run in the NUS mode. Up to now, XCloud-MoDern uses model-inspired deep learning (MoDern) to fast recover high-quality multi-dimensional spectra from NUS data, and also provides a customized retrospectively undersampling technique (NUS simulator) to produce NUS data and the corresponding NUS mask from the fully sampled NMR data. The pre- and post- processing are done in NMRPipe<sup>[9]</sup>, which is a generic spectral processing engine in NMR, to meet diverse demands of users and enhance the universality of our cloud platform. In the cloud, besides deploying the above-mentioned data processing methods (MoDern and NUS simulator), many other files such as the user manual, demonstration data and scripts, and trained network weights are stored.

To ensure the efficiency of the platform, the configuration of the China Mobile e-cloud host is as follows: 8 cores CPU, 64 GB RAM, one Nvidia T4 GPU, and 500 GB SSD. The reconstruction time on cloud using MoDern is reported in Table S8-1, which is highly consistent with Table S7-1.

Details on the instructions of XCloud-MoDern are described in its manual available on our cloud platform, and you can find it at <https://github.com/wangziblake/MoDern>. We have provided some demo data and scripts on the cloud for the quick try. The screenshots of XCloud-MoDern can be found in Figure S8-1 and S8-2.

**Table S8-1.** Reconstruction time on cloud using MoDern (Unit: seconds). For 2D (3D) spectra, the size of the directly detected dimension is followed by the size(s) of the indirect dimension(s).

Spectra Type		Samples	Molecular weight	Spectra size	Reconstruction time on cloud
					XCloud-MoDern
2D	HSQC	CD79b	5.7 kDa	116 × 256	<b>0.37</b>
	HSQC	Gbl	8.0 kDa	1146 × 170	<b>0.42</b>
	TROSY	Ubiquitin	8.6 kDa	512 × 128	<b>0.39</b>
	NOESY	Ubiquitin	7 kDa	928 × 512	<b>0.55</b>
3D	HNCACB	GB1-HttNTQ7	10 kDa	879 × 90 × 44	<b>2.50</b>
	HNCO	Azurin	14 kDa	732 × 60 × 60	<b>1.97</b>
	HNCO	MALT1	44 kDa	735 × 57 × 70	<b>3.09</b>
	HNCO	Alpha-synuclein	14.5 kDa	221 × 64 × 64	<b>0.94</b>

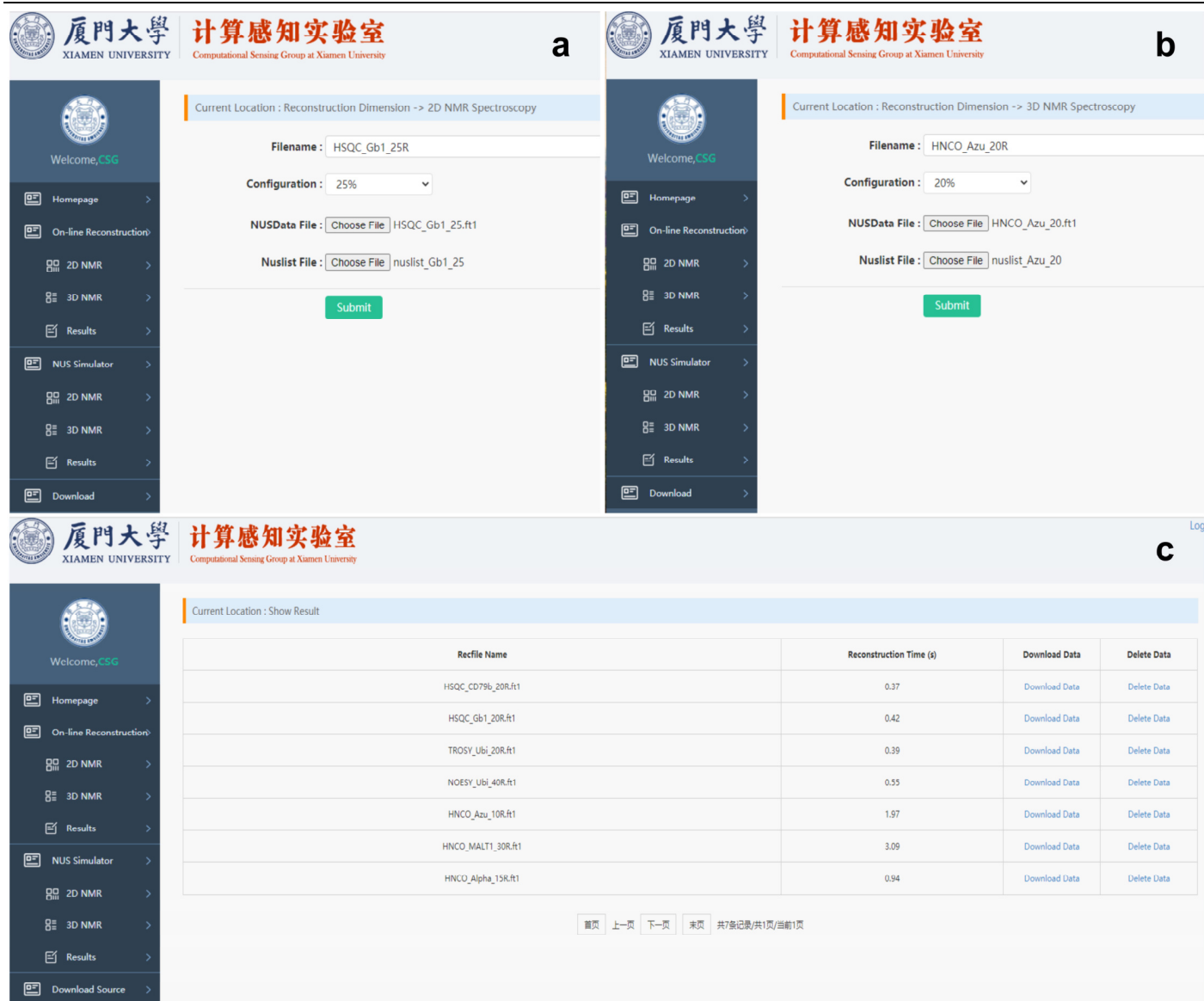


**Figure S8-1.** The screenshots of on-line reconstruction webpages of XCloud-MoDern. (a) and (b) are on-line reconstruction webpages for 2D and 3D NMR data reconstruction using MoDern. (c) is the webpage for downloading reconstructed results and checking the reconstruction time. (e) and (f) are customized retrospectively undersampling webpages for 2D and 3D NMR data using NUS simulator. (g) is the webpage for downloading the NUS data and the corresponding NUS mask.



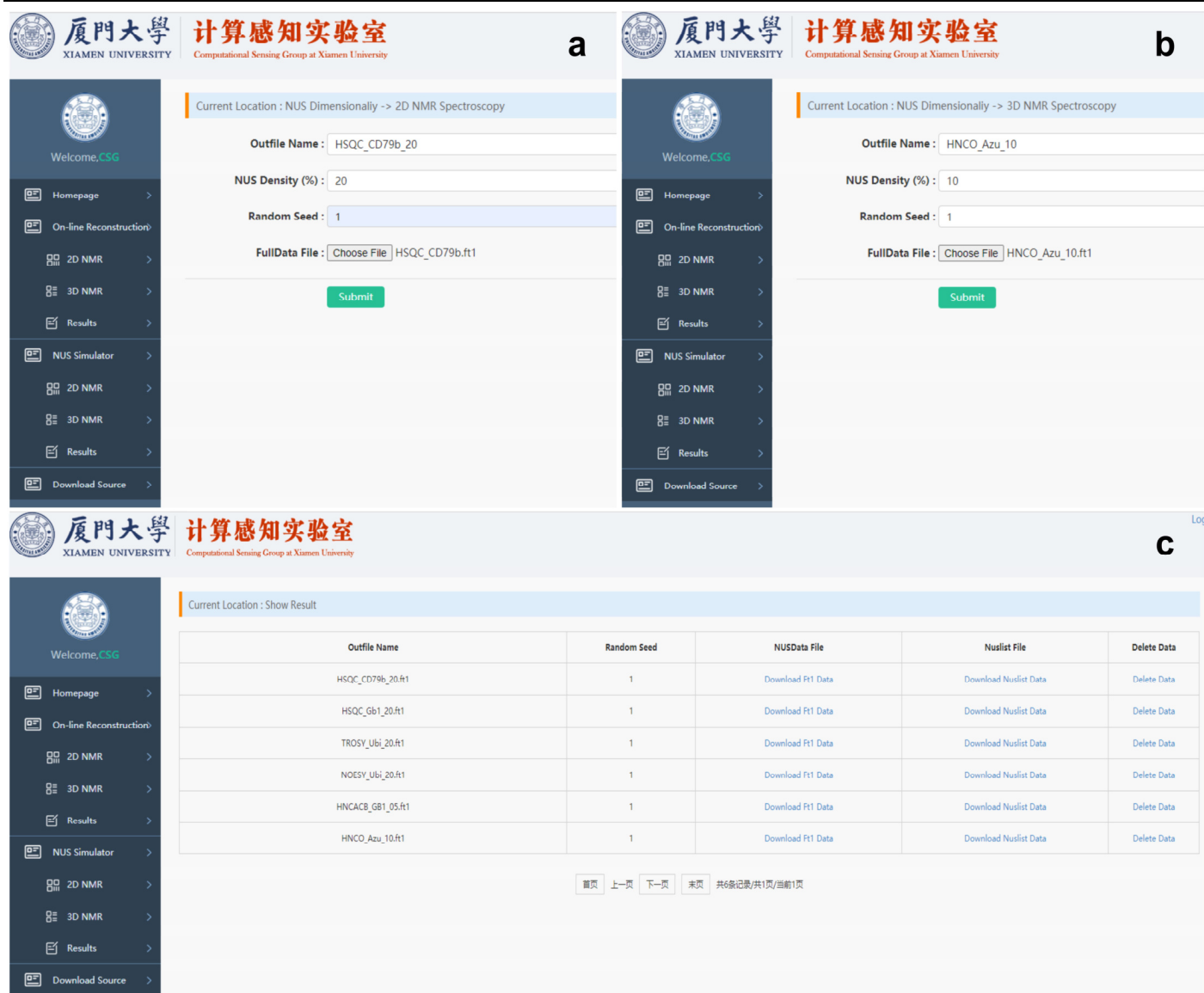


**Figure S8-2.** The screenshots of customized retrospectively undersampling webpages of XCloud-MoDern. (a) and (b) are customized retrospectively undersampling webpages for 2D and 3D NMR data using NUS simulator. (c) is the webpage for downloading the NUS data and the corresponding NUS mask.

---

## References

- [1] X. Qu, Y. Huang, H. Lu, T. Qiu, D. Guo, T. Agback, V. Orekhov, Z. Chen, *Angew. Chem. Int. Ed.* **2020**, *59*, 10297-10300.
- [2] a) J. Hoch, A. Stern, *NMR data processing*, **1996**; b) X. Qu, M. Mayzel, J.-F. Cai, Z. Chen, V. Orekhov, *Angew. Chem. Int. Ed.* **2015**, *54*, 852-854.
- [3] S. G. Hyberts, K. Takeuchi, G. Wagner, *J. Am. Chem. Soc.* **2010**, *132*, 2145-2147.
- [4] M. Mayzel, K. Kazimierczuk, V. Y. Orekhov, *Chem. Commun.* **2014**, *50*, 8947-8950.
- [5] a) K. Kazimierczuk, V. Y. Orekhov, *Angew. Chem. Int. Ed.* **2011**, *50*, 5556-5559; b) S. G. Hyberts, A. G. Milbradt, A. B. Wagner, H. Arthanari, G. Wagner, *J. Biomol. NMR* **2012**, *52*, 315-327.
- [6] D. Chen, Z. Wang, D. Guo, V. Orekhov, X. Qu, *Chem. –Eur. J.* **2020**, *26*, 10391-10401.
- [7] K. He, X. Zhang, S. Ren, J. Sun, *arXiv preprint arXiv:1502.01852* **2015**.
- [8] D. Kingma, J. Ba, *arXiv preprint arXiv:1603.04467* **2014**.
- [9] F. Delaglio, S. Grzesiek, G. W. Vuister, G. Zhu, J. Pfeifer, A. Bax, *J. Biomol. NMR* **1995**, *6*, 277-293.
- [10] S. A. Kotler, V. Tugarinov, T. Schmidt, A. Ceccon, D. S. Libich, R. Ghirlando, C. D. Schwieters, G. M. Clore, *P. Natl. Acad. Sci. USA* **2019**, *116*, 3562-3571.
- [11] S. Unnerst  le, M. Nowakowski, V. Baraznenok, G. Stenberg, J. Lindberg, M. Mayzel, V. Orekhov, T. Agback, *PLoS One* **2016**, *11*, e0146496.
- [12] Y. Pustovalova, M. Mayzel, V. Y. Orekhov, *Angew. Chem. Int. Ed.* **2018**, *57*, 14043-14045.
- [13] S. G. Hyberts, S. A. Robson, G. Wagner, *J. Biomol. NMR* **2013**, *55*, 167-178.
- [14] a) Y. Huang, J. Zhao, Z. Wang, D. Guo, X. Qu, *arXiv preprint arXiv:2007.06246* **2020**; b) D. F. Hansen, *J. Biomol. NMR* **2019**, *73*, 577-585.
- [15] K. Hu, W. M. Westler, J. L. Markley, *J. Am. Chem. Soc.* **2011**, *133*, 1662-1665.
- [16] M. Abadi, A. Agarwal, P. Barham, E. Brevdo, Z. Chen, C. Citro, G. Corrado, A. Davis, J. Dean, M. Devin, S. Ghemawat, I. Goodfellow, A. Harp, G. Irving, M. Isard, Y. Jia, R. Jozefowicz, L. Kaiser, M. Kudlur, X. Zheng, *arXiv preprint arXiv:1603.04467* **2016**.
- [17] W. Lee, M. Tonelli, J. L. Markley, *Bioinformatics* **2015**, *31*, 1325-1327.

## Author contributions

X. Qu and Z. Wang conceived the idea and designed the study, X. Qu supervised the project, Z. Wang, Z. Tu, and Y. Huang implemented the method and produced the results, Z. Wang drew all the figures for the manuscript and supporting information, Y. Zhou, J. Wang, and Z. Wang developed the cloud computing platform, L. Feng and D. Lin acquired one 2D NMR data of a mixture. Y. You provided China Mobile ecloud computing service support. T. Agback acquired one 3D NMR data of a large protein. The manuscript was drafted by Z. Wang and improved by Z. Wang, D. Guo, Z. Tu, V. Orekhov, and X. Qu. X. Qu and D. Guo acquired research funds and provided all the needed resources.